SANDIA REPORT
SAND2006-7239
Unlimited Release
Printed November 2006

Laser Based Micro Forming and Assembly

Jeremy A. Palmer, Gerald A. Knorovsky, Danny O. MacCallum, Michele Steyskal, William M. Scherzinger, C. Channy Wong, and Tom M. Lehecka

Prepared by
Sandia National Laboratories
Albuquerque, New Mexico 87185 and Livermore, California 94550

Sandia is a multiprogram laboratory operated by Sandia Corporation,
a Lockheed Martin Company, for the United States Department of Energy's
National Nuclear Security Administration under Contract DE-AC04-94AL85000.

Sandia National Laboratories

Issued by Sandia National Laboratories, operated for the United States Department of Energy by Sandia Corporation.

Available to DOE and DOE contractors from
U.S. Department of Energy
Office of Scientific and Technical Information
P.O. Box 62
Oak Ridge, TN 37831

Telephone: (865) 576-8401
Facsimile: (865) 576-5728
E-Mail: reports@adonis.osti.gov
Online ordering: http://www.osti.gov/bridge

Available to the public from
U.S. Department of Commerce
National Technical Information Service
5285 Port Royal Rd.
Springfield, VA 22161

Telephone: (800) 553-6847
Facsimile: (703) 605-6900
E-Mail: orders@ntis.fedworld.gov
Online order: http://www.ntis.gov/help/ordermethods.asp?loc=7-4-0#online

SAND2006-7239
Unlimited Release
Printed November 2006

Laser Based Micro Forming and Assembly

Jeremy A. Palmer
Meso Manufacturing and System Development Department

Gerald A. Knorovsky
Joining and Coating Department

Danny O. MacCallum
Joining and Coating Department

Michele Steyskal
Explosive Projects/Diagnostics Department

William M. Scherzinger
Solid Mechanics Department

C. Channy Wong
Microscale Science and Technology Department

Sandia National Laboratories
P.O. Box 5800
Albuquerque, NM 87185-1064

Tom M. Lehecka
Pennsylvania State University Electro Optics Center
Freeport, PA, 16229

Abstract

It has been shown that thermal energy imparted to a metallic substrate by laser heating induces a transient temperature gradient through the thickness of the sample. In favorable conditions of laser fluence and absorptivity, the resulting inhomogeneous thermal strain leads to a measurable permanent deflection. This project established parameters for laser micro forming of thin materials that are relevant to MESA generation weapon system components and confirmed methods for producing micrometer displacements with repeatable bend direction and magnitude. Precise micro forming vectors were realized through computational finite element analysis (FEA) of laser-induced transient heating that indicated the optimal combination of laser heat input relative to the material being heated and its thermal mass. Precise laser micro forming was demonstrated in two practical manufacturing operations of importance to the DOE complex: micrometer gap adjustments of precious metal alloy contacts and forming of meso scale cones.

Acknowledgment

The authors thank Sandia National Laboratories staff members Josh Arvizu, Juan Romero, Rosa Montoya, Nolan Finch, and Frank Peter for their contributions to this research. Additional thanks to students Fred Livingston (North Carolina State University) and Gustavo Roman (The University of Florida). Lastly, the authors acknowledge Honeywell FM&T staff members Tim Castillo and Matthew Wiloughby for their guidance in manufacturing systems development.

Contents

Figures

Tables

Laser Based Micro Forming and Assembly

Jeremy Palmer, Jerry Knorovsky, Danny MacCallum, Michele Steyskal, Bill Scherzinger, Channy Wong, Tom Lehecka

1.0 Introduction

Complex mechatronic products in the aerospace, automotive, and defense markets have evolved to satisfy ever-changing demands for greater functionality, performance, safety, reliability, and economy. This trend has fueled technical achievements in material and manufacturing systems, many of which are related to miniaturization. Beyond the domain of semiconductor microfabrication, the methods we use to create and assemble miniature or *meso* electromechanical components with micrometer features and precise tolerances have also improved (Gilbert, 1961; Kang, Lee, and Prinz, 2001)[1, 2]. Some traditional methods have been adapted to smaller scales. One example is thermal forming (so-called flame bending) of metals (Magee, Watkins, and Steen, 1998)[3]. Before the 1990's, flame bending was applied more frequently in heavy industries such as ship building and construction[3]. Over the past decade however, knowledge of flame bending has led to laser forming (LF) and, more recently, laser micro forming of metals (Vollertsen, Hu, Schulze Neihoff, Theiler, 2004)[4, 3]. Laser micro forming has been successfully applied to create micrometer bends or adjustments in miniature metal components such as reed switch contacts and disk drive read/write heads (Schmidt, Dirshcerl, Rank, and Zimmermann, 2005; Hoving, 2003)[5, 6]. This paper reports research to advance laser micro forming of small, thin precious metal substrates and meso scale conical forms. Laser micro forming is the foundation for a disruptive meso manufacturing system including large deflection of metallic links, laser welding, and laser machining that enables component assembly without fasteners or human intervention.

1.1 Mechanisms for Laser Forming of Metals

Several unique laser forming mechanisms have been observed and analyzed[3]. The majority are thermo-mechanical[3]. However, shock wave micro forming using ultra short laser pulses is also possible (Dirscherl, Esser, and Schmidt, 2006)[7]. Most relevant to this investigation is the Thermal Gradient Mechanism (TGM) and the Buckling Mechanism (BM), both proposed by Vollertsen (Vollertsen, 1994; Vollertsen, Komel, and Kals, 1995)[8, 9, 3]. As Fig. 1 illustrates, the TGM models transient laser heating of a homogeneous unsupported substrate whose thickness S_0

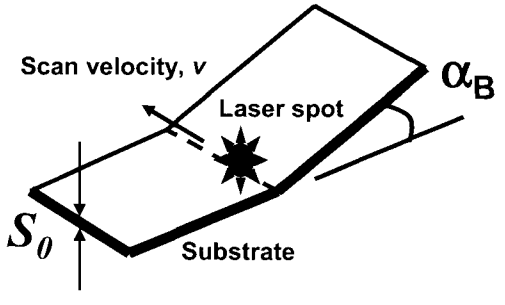

Fig. 1. Thermal gradient induced by laser heating of a metallic substrate[3].

is divided in two layers[3, 8]. In Fig. 1, the laser focal spot is scanned with velocity v across the top surface of the substrate as shown[3, 8]. Thermal energy imparted to the substrate by laser heating induces a transient temperature gradient through the thickness. In favorable conditions of laser fluence and absorptivity, the resulting inhomogeneous thermal strain leads to a measurable permanent deflection (angle α_B, see Fig. 1)[3, 8]. Initial laser heating causes the upper layer of the substrate to expand, thus causing it to bend away from the focal spot[3, 8]. As the temperature of the upper surface rises, the elasticity decreases, and the substrate can no longer resist the stress from the initial bend[3, 8]. The result is a subsequent bend in the opposite direction *toward* the focal spot which increases when the laser is removed and cooling ensues. The final result is a net bend toward the spot[3, 8]. Net bending is expressed by the following:

$$\alpha_B = 3\frac{\alpha_{th} P_1 A}{\rho c_p v S_0^2} \tag{1}$$

where α_{th} is the coefficient of thermal expansion of the substrate material, P_1 is the laser power, A is the absorption coefficient, ρ is the substrate density, and c_p is the constant pressure specific heat of the substrate material[8]. Although it provides a reasonable estimate, the equation (1) does not account for the initial bend away from the focal spot and consequently overestimates the bend angle[3]. Yau, Chan, and Lee derived a version of the TGM model that accounts for the initial bend (Yau, Chan, and Lee, 1997)[10]. By the Yau model, the expression for the net bending becomes:

$$\gamma = \left(\frac{7}{2}\right)\frac{3\alpha_{th} P_1 A}{\rho c_p v S_0^2} - 36\frac{l\sigma_y}{S_0 E} \tag{2}$$

where l corresponds to the radius of the laser spot, σ_y is the substrate material yield stress, and E is the modulus of elasticity[10]. The BM may dominate in meso and microsystems applications where a thin substrate with a high ratio of thermal conductivity to thickness is slowly scanned by a large (relative to the thickness) spot[3, 9]. In this case, buckling instability may cause the direction of bending to be random[3, 9]. Moreover, the direction of bending can be biased by boundary conditions such as the configuration of substrate supports and residual stress[3, 10]. By the BM model, the magnitude of net bending is written as:

$$\alpha_B = \left[36\frac{\alpha_{th} k_f(T) P_1 A}{\rho c_p E v S_0^2}\right]^{\frac{1}{3}} \tag{3}$$

where $k_f(T)$ is the temperature dependent flow stress[9]. In practice, the TGM and BM models provide reasonable estimates of net bending provided the assumptions are valid. Other situations require a numerical approach.

1.2 Numerical Simulations

Laser based micro forming is modeled with a coupled thermo-mechanical finite element code – Calagio. Calagio couples the thermal analysis code Calore with the quasi-static solid mechanics code Adagio. Both codes are developed in the SIERRA framework, a software environment for developing complex multi-physics applications. The SIERRA framework and the analysis codes Calore and Adagio were developed at Sandia National Laboratories' Engineering Sciences Center.

1.2.1 Thermal Analysis

Calore is a computational program for transient three-dimensional heat transfer analysis. It is built upon the SIERRA finite element framework to run on both desktop and parallel computers. Advanced thermal analysis capabilities include anisotropic conduction, enclosure radiation, thermal contact, and chemical reaction. The governing energy conservation equation in Calore is expressed as follows:

$$\frac{\partial}{\partial t}(\rho \cdot c \cdot T) + \sum_{i=x,y,z} \frac{\partial}{\partial x_i}(\rho \cdot c \cdot u_i \cdot T) = \sum_{i=x,y,z} \frac{\partial}{\partial x_i}(q_i) + S \tag{4}$$

where

$$q_i = -\sum_{j=x,y,z} k_{ij} \frac{\partial T}{\partial x_j} \tag{5}$$

and ρ is density, c is heat capacity, T is temperature, u_i is convective velocity, q is heat flux, and S is the volumetric heat generation rate. Boundary conditions available include specified temperature, heat flux, force or free convection, and surface radiation. Calore also has many state-of-the-art computational features such as element death, automatically selection of the time step size, mesh adaptivity, and dynamic load balancing for massively parallel computing.

1.2.2 Solid Mechanics Analysis

Adagio is a nonlinear quasi-static finite element code. It uses an iterative nonlinear preconditioned conjugate gradient method for the solution algorithm. Adagio solves problems using an incremental solution algorithm – the analysis is divided up into a number of time steps and the incremental solution for the problem is found for each time step. This approach is ideal for solving problems with geometric and material nonlinearities. A conjugate gradient solution algorithm needs a preconditioner for the problem, and the particular preconditioner that is chosen along with a number of parameters that affect the solution algorithm can have a large effect on the convergence behavior of the code. Adagio is fully capable of handling finite deformation kinematics. In addition to nonlinear geometrical terms, it also has a suite of nonlinear constitutive models that are capable of modeling a wide range of material behavior, including rubber elasticity, metal plasticity and polymer viscoelasticity to name a few.

The problems examined for laser based micro forming are, from a solid mechanics perspective, principally structural. The laser bending model discussed here is essentially a beam bending problem while the cone forming problem involves the deformation of a disk. Both problems compute finite deformations of thin structures. Because of this a full-tangent preconditioner is used for the solution algorithm in Adagio. Other choices are not good for finding the structural response that we expect in both problems.

FETI – the Finite Element Tearing and Interconnecting algorithm – is used for these problems. This dramatically reduces the iterations per increment when compared with a nodal

based preconditioning algorithm. The full tangent preconditioner is a better choice than the nodal based preconditioner for structural problems like those seen in laser based micro forming.

A solution parameter that can have a large effect on the convergence is the predictor scale factor. Put simply, a predictor attempts to predict the incremental solution for a given time step. In the case of a small deformation problem, each solution step will have similar solutions. Therefore, using the last incremental solution as the predicted solution for the next time step is usually a good approach for this type of problem. Even though the displacements are relatively large – resulting in a geometrically non-linear problem – incrementally the displacements are usually small.

Numerical solutions for the quasi-static analysis of a structural problem, like those examined for laser based micro forming, are most easily found using the full-tangent preconditioner and the predictor scale factor. Modifying their use during various solution periods aids in the convergence of the problem. These modifications have no effect on the accuracy of a solution except in cases where a solution will not converge unless the proper numerical scheme is used.

Since the prediction of permanent deformation depends on the accumulation of plastic deformation, the constitutive model is important in modeling laser based micro forming. For the analyses that are run for this study, elastic-plastic power law hardening models are used. In addition the models are temperature dependent – another requirement on the constitutive model given the application. The constitutive model is the same for all materials used in this study – but the parameters, or material properties, are different. Given the nature of the study this is considered a good first approximation of the material behavior. Furthermore, the hardening behavior goes beyond what is generally found in the literature. The actual constitutive model and the parameters for alloys used in this study (Neyoro-G™ and 304L stainless steel) will be presented in a later section.

Finally, the solid mechanics models are also dependent on the boundary conditions. Since the problem with the cantilever beam strip involves an initial displacement, modeling this correctly is crucial to the solution of the problem. With the cone forming problem, boundary conditions have less influence. For the mechanical response of the disk all boundaries are assumed to be traction free.

1.3 Effects of Substrate Thickness and Stress Condition

Many published investigations of laser metal forming measure bend angle in substrates with constant or varying thickness greater than 1 millimeter (Cheng *et al.*, 2006; Walczyk and Vittal, 2001)[11, 12, 3, 7, 8]. Although the definition varies among authors, the term "thin" for the purpose of this paper denotes substrate thickness that is 1 mm or less. Lee and Lin modeled forming with a stationary pulsed laser beam and elliptical focus incident on stainless steel substrates with thickness ranging from 1.5 to 0.5 millimeters (Lee and Lin, 2002)[13]. For laser heating with 100 millisecond pulses, they observed that the bend angle is directly proportional to laser power and inversely proportional to substrate thickness[13]. The direction of bending was consistently (upward) toward the laser beam[13]. However, bending in the opposite direction was noted in the case of laser irradiation at high power and pulse duration where the peak temperature exceeded the material melting point[13]. Kals and Vollertsen observed a reduction in maximum bending force in laser-irradiated copper alloy sheets with thickness less than 0.5 millimeters[4]. They noted that the force reduction was less pronounced in samples with larger grains[4].

Vollertsen discussed the influence of the stress state of the substrate on the direction of laser bending[9]. Where bending is driven by the BM, applied elastic stress or relaxation of residual

stress in the substrate causes the direction of bending to be deterministic[9]. More important to this investigation, the bend direction remains random in cases where a plastic stress is pre-applied (from a prior conventional cold forming operation, for example)[9]. This hypothesis was partially validated by the work of Yanjin *et al.* (Yanjin *et al.*, 2003)[14]. Considering a cantilever steel sheet, they demonstrated how elastic deflection applied prior to laser irradiation results in bending with consistent direction[14].

1.4 Precious Metal Alloys

To date, validation data for analytical models exists for a limited group of common metals, including stainless steels, titanium, and chromium (Dearden and Edwardson, 2003)[15, 3, 8, 9, 12]. Numerical analysis by Yanjin *et al.* predicted that bending angle is inversely proportional to thermal conductivity (Yanjin *et al.*, 2005)[16]. Moreover, inspection of (1-3) also reveals that bending angle is also inversely proportional to specific heat. Consequently, it is reasonable to assume that laser bending in precious metal alloys with high thermal conductivity and specific heat capacity may be more difficult to achieve.

Neyoro-G™ is a commercial gold-copper-platinum alloy with high electrical and thermal conductivity (Deringer-Ney, 2006)[17]. Laser micro forming of thin Neyoro-G™ strips was studied in this program. Material properties are listed in Table 1. Figure 2 is a reflectivity

Table 1. Material Properties of Neyoro-G™ Annealed Strip[17]

Property	Value	Units
Elastic modulus	16 x 10^3	ksi
Proportional limit	65	ksi
Ultimate tensile strength	85-115	ksi
Coeff. of thermal expansion	12.6	ppm/°C
Density	0.574	lbm/in^3

spectrum of Neyoro-G™ relative to a silver standard. Note the discontinuity in the reflectivity at 900 nm is a consequence of the different optical filters used in the radiometer analysis.

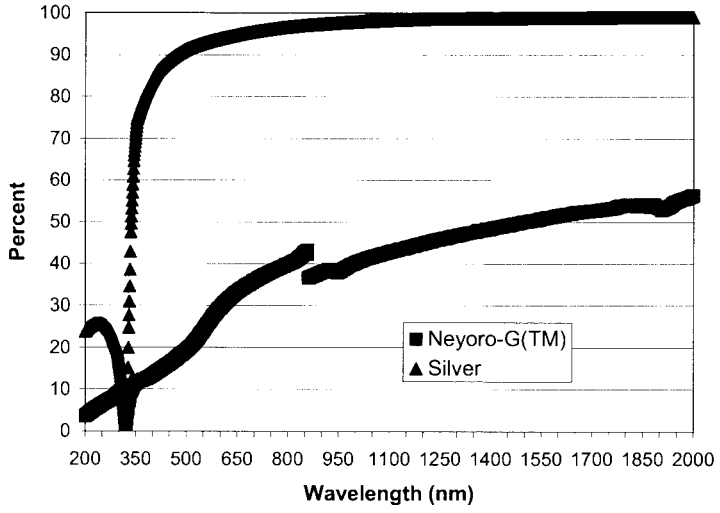

Fig. 2. Neyoro-G™ reflectivity vs. wavelength

1.5 Micro Forming of Electrical Contacts

Increasing research has been devoted to applications of laser micro forming in microsystems manufacturing in recent years[4, 5, 6]. Relatively little has been published on laser micro forming of precious metal alloys in electrical and electronic systems. A familiar problem in the context of electrical contacts involves micrometer adjustments of the gap between a pair of opposing contacts with micrometer or sub-micrometer precision[5, 6]. A widely known example is so-called laser micro adjustment of opposing nickel-iron contacts in enclosed magnetic reed switches[5, 6]. In many similar products, accuracy and precision of the contact gap has a significant impact on performance and reliability.

Fig. 3 illustrates the contact gap problem at the center of this investigation. In manufacturing

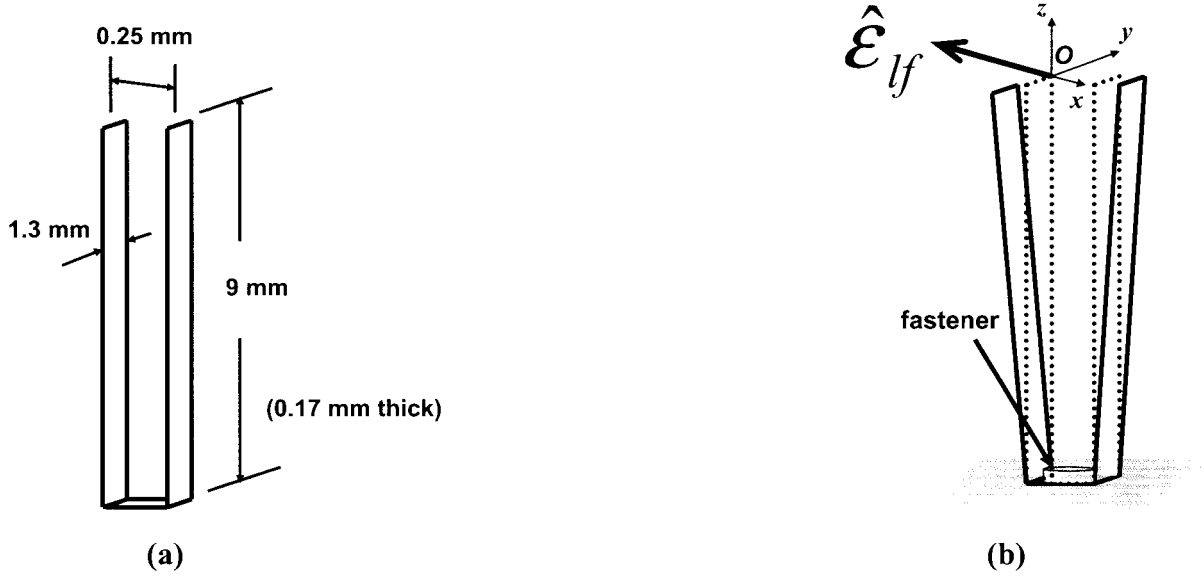

Fig. 3. Geometry of electrical contacts: (a) Nominal, (b) After fastening operation.

assemblies of gold-copper alloy contacts for an electrical product, the legs of individual contacts incur plastic deformation in the fastening operation (see Fig 3(b)). It follows that the contact gap increases and ultimately exceeds the product specification (see Fig. 3). The contact gap, which is crucial to product performance, must subsequently be adjusted to compensate. Manual adjustment is incapable of setting the gap with the desired 50 micrometer accuracy. A forming vector is defined as follows:

$$\hat{\varepsilon}_{lf} = \varepsilon_{lf}\left(\cos\theta_x \hat{i} + \cos\theta_y \hat{j} + \cos\theta_z \hat{k}\right). \tag{6}$$

where θ_x, θ_y, and θ_z are angles measured from a Cartesian coordinate system at the tip of the contact point O as shown in Fig. 3(b) and $\hat{i}$, $\hat{j}$, and $\hat{k}$ are unit vectors. An effective laser micro forming process controls the magnitude and sense (direction) of the forming vector (6).

Laser micro forming of Neyoro-G™ was achieved in 2006 by Lehecka, Campbell, and Campbell (Lehecka, Campbell, and Campbell, 2006)[18]. In that study, a GSI Lumonics JK702H laser operating at 1064nm (120 millisecond pulses) was used to bend Neyoro-G™ cantilevers corresponding to the dimensions shown in Fig. 3(a). Laser bends ranged from 50 micrometers in the downward direction to 500 micrometers upward (toward the source of the beam and against gravity). Micro forming was observed with single-pulse irradiation of the sample over a range of 4 to 7 Joules per pulse. At low pulse energy, the sample would randomly bend up or down by tens of microns or less. As energy was increased, the bending became consistently upward with deflections of 50 micrometers or greater. As energy was increased further, samples tended to melt and lose their rigidity. It follows that to enable micro bending at low pulse energies, a pre-applied bias is necessary to make the sense or direction of the forming vector deterministic. This is discussed in detail in a later segment.

1.6 Conical Forms

Conical shaped charges are explosive devices which form a jet from the cone material that then penetrates into another target material. Some conical shaped charges are used for purposes where the penetration depth isn't critical; however, in many cases the penetration must be a specific value with a tight tolerance. In the latter case, the shaped charge must act as a precision device. As with any precision device, it becomes important how the parts of the device are manufactured. With a shaped charge, the cone must be manufactured to high standards to obtain a repeatable amount of penetration.

Many methods have been used to manufacture shaped charge cones such as stamping and machining. Depending on the size of the shaped charge, each method has pros and cons. For small, meso scale shaped charges, stamping the cones usually produces the best results. However, stamping can be an expensive process, and making design changes is difficult because new dies must be created. Machining meso scale cones is another option. However, even though machining can produce cones with small dimensional tolerances, normally the resulting cones do not have a smooth enough finish. Even small machining grooves can cause the jet to become a spiral instead of a straight uniform shape. This issue becomes more apparent as the cone gets smaller in size. Machining the cones does have benefits however because design changes are simple and only making a few cones at a time is not an issue.

An optimal manufacturing process for meso scale shaped charge cones would include flexibility for design changes, smooth reproducible cones, and cost effectiveness. Currently, a meso scale shaped charge with nuclear weapons connections is in need of both a redesign and a reliable way to make the cones. Fig. 4 shows the general dimensions of this specific shaped charge cone. Stamping is not ideal during a redesign since making multiple dies for new designs is expensive. As stated earlier, machining is not ideal since it can cause spiral jets and non reproducible penetration results. However, laser forming would be an ideal candidate since it could produce cones with a smooth finish like stamping, but provide the flexibility of changing the design without expensive dies. Furthermore, this specific shaped charge is smaller than most other shaped charges so it has unique manufacturing issues. Laser forming should be able to address these unique manufacturing issues.

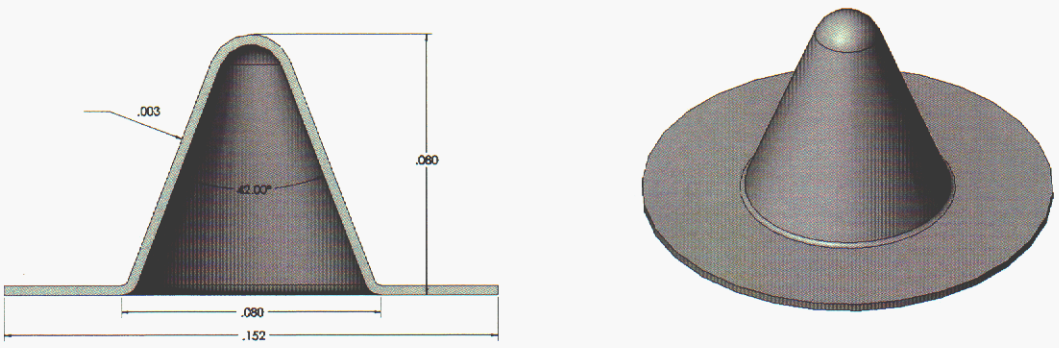

Fig. 4. Shaped charge cone generalized dimensions.

Metal spinning is a forming process that is typically done on a lathe to produce round hollow metal forms. It is the primary alternative to expensive sheet metal stamping machinery. The flat sheet of metal is attached to a mandrel and rotated at very high speeds. The shape of the mandrel will determine the final shape of the sheet metal. As the metal is spinning a levered force is applied. This force is uniform due to the spinning and allows the metal to deform evenly without wrinkling. Due to work hardening it is sometimes necessary to anneal the sheet metal during the process. Depending on the complexity of the final shape, this process can be labor intensive and difficult if done manually. State of the art facilities have computer numeric controlled spinning machines.

While metal spinning is the predominant method to produce bowl and conical shapes, there has been an exploration into applying laser forming techniques to achieve these geometries. The controlled generation of complex curved sheet metal parts was investigated by Hennige (Hennige, 2000)[19]. Insight was obtained in the differences between straight and curved irradiation paths, sighting a strong influence from the material adjacent to the irradiated area. This was done by comparing results of experiments performed on square and circular sections with the same characteristic dimensions. The author also explored the relationship between number of irradiations and bend angle. A significant step was made with the idea of using both radial and concentric irradiation paths on the same piece of metal. This concept was coupled with the changing of laser parameters to induce either TGM or BM, for the radial and concentric paths respectively. The described method produced a spherical dome from a flat circular piece of sheet metal. The experiments on laser forming of circular sections showed a significant reduction in achievable bend angle when compared to linear laser bending[19]. Casalino *et al.* also explored the production of complex shapes generated using a curved-path irradiation strategy, focusing on circular plates of sheet metal (Casalino and Ludovico, 2003)[20]. They were able to highlight the interactions between certain process parameters. In particular the authors cite a high relationship between laser power and running speed. They remark that 304 stainless steel shows good laser formability. The authors used experimental results to validate their numerical model, claiming agreement within 2% of experimental results. The authors also list specific operating process parameters to be optimized.

1.7 Research Objectives

A research program was conceived to investigate micro laser forming in two value-added manufacturing applications. The first is contact gap adjustment. The second is a novel approach to creating meso conical forms.

In the first application, micro laser forming was investigated as an alternative to manual manipulation in gap adjustment of Neyoro-G™ electrical contacts (see Fig. 3(a)). The objective of the study was to achieve a desired micro forming vector in single pulse irradiation of a Neyoro-G™ strip with cantilever end constraint as shown in Fig. 5. Length L and other

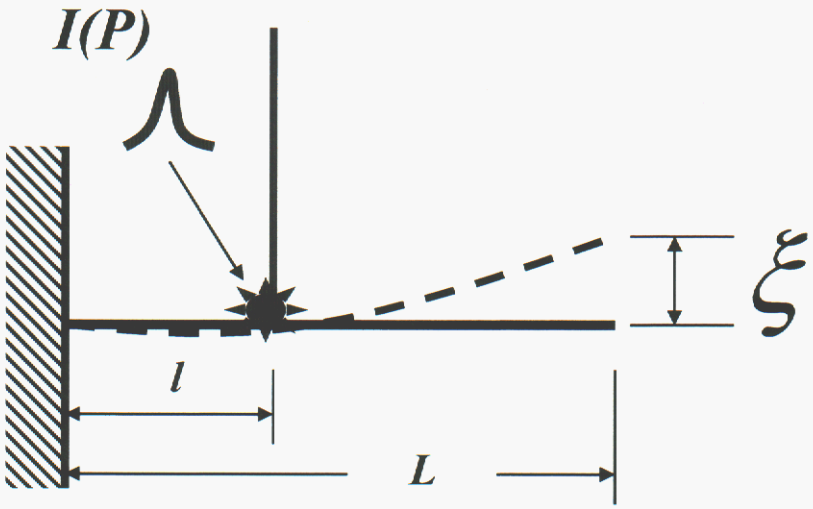

Fig. 5. Neyoro-G™ cantilever configuration for laser micro forming study.

dimensions are given in Fig. 3(a). The magnitude of the desired vector is 25 micrometers measured at the tip of one contact leg as shown in Fig. 3(b). The sense or direction of the vector must be deterministic and consistent. To realize this objective, a deflection ξ was pre-applied at the tip to bias the system in one direction. This study is unique in that it is (to the authors' knowledge) the first comprehensive study of laser micro forming in a precious metal alloy such as Neyoro-G™ that considers effects of pre-applied elastic stress.

This work also introduces the concept of *micro laser spinning* of conical forms. Micro laser spinning combines laser micro forming with metal spinning to realize 304L stainless steel meso cones with unprecedented apex angles (see Section 1.6, above). The conjecture is that rotating the work piece may aid the micro forming operation by the contribution of axisymmetric, dynamically-induced plastic strain. Results of a FEA of the stationary disk are applied to determine parameters for laser irradiation of a meso disk that is rotated in a motorized spinning apparatus.

2.0 Formulation of Numerical Simulations

The temperature dependent elastic-plastic power law hardening constitutive model is applied to both the Neyoro-G™ and 304L stainless steel systems described here. The model uses a standard radial return algorithm for computing the material state. This state is given by the equivalent plastic strain and the back stress for the material. Since isotropic hardening is used in both models, the back stress is always zero and the equivalent plastic strain uniquely determines the state. The equivalent stress-equivalent plastic strain curve for the model has the form

$$\bar{\sigma} = \sigma_y + A\left\langle \bar{\varepsilon}_p - \varepsilon_l \right\rangle^n , \tag{7}$$

where σ_y is the yield stress, $\bar{\varepsilon}_p$ is the equivalent plastic strain, A is the hardening constant, n is the hardening exponent and ε_l is the Luder's strain. The model is temperature dependent – a requirement given the problems we are solving. The material properties in the model – specifically the Young's modulus, Poisson's ratio and yield stress – are dependent on temperature. Since there is little data available on the variation of the Poisson's ratio with temperature, this is assumed constant for both materials. The Young's modulus and yield stress as functions of temperature are determined from experimental data.

The material data for Neyoro-G™ was found from two sources. Some of the material properties are those for gold, e.g. the density and Poisson's ratio. Others were found from experimental data generated in organization 1824. Data for 304L stainless steel was found from experimental data generated for other programs.

The material properties for the temperature dependent elastic-plastic power law hardening model for both the Neyoro-G™ and 304L stainless steel are given in Table 2.

Table 2. Material Properties for Power Law Hardening Model at Room Temperature

Property	Neyoro-G™	304L stainless steel
Young's modulus (E - dyne/cm^2)	1.1×10^{12}	1.93×10^{12}
Poisson's ratio (ν)	0.44	0.30
yield stress (σ_y - dyne/cm^2)	5.5×10^{9}	2.27×10^{9}
hardening constant (A - dyne/cm^2)	3.35×10^{9}	7.29×10^{9}
hardening exponent (n)	0.3	0.49
Luder's strain (ε_l)	0.0	0.0
Beta (β)	1.0	1.0

The temperature dependence is found through scaling functions for the Young's modulus and the yield stress. For Neyoro-G™ these functions are in Table 3. Parameters for 304L stainless steel are given in Tables 4 and 5.

Table 3. Scale Factors for Young's Modulus and Yield Stress as a Function of Temperature for Neyoro-G™

Temperature (K)	Young's Modulus Scale Factor	Yield Stress Scale Factor
293	1.00	1.00
373	1.00	1.56
473	0.95	1.46
573	0.88	1.08
673	0.70	0.60
773	0.33	0.21
873	0.17	0.08

Table 4. Scale Factor for Yield Stress as a Function of Temperature for 304L Stainless Steel

Temperature (K)	Yield Stress Scale Factor
33	1.30
89	1.27
144	1.22
200	1.15
255	1.07
293	1.00
311	0.98
367	0.86
423	0.75
477	0.68
533	0.64
589	0.62
645	0.62
700	0.62
755	0.62
811	0.61
866	0.58
922	0.55
978	0.50
1033	0.44
1081	0.39

Table 5. Scale Factor for Young's Modulus as a Function of Temperature for 304L Stainless Steel

Temperature (K)	Young's Modulus Scale Factor
293	1.00
311	1.00
421	1.00
533	0.96
644	0.89
755	0.86
866	0.79
977	0.71
1089	0.64

2.1 Electrical Contacts

This section addresses formulating the models in Calagio to analyze the Neyoro-G™ cantilever experiment performed at the Pennsylvania State University Electro Optics Center (see Section 3.1). The development of a computational model and the setup to simulate the testing procedures as in the experiment will be covered. Calagio prediction of the permanent deflection at the tip of the cantilever will be compared with the experimental measurement and results will be discussed in Section 4.1. Our goal is to validate the computational models in Calagio and to build confidence of further applying the code to investigate the thermo-mechanical responses of Neyoro-G™ cantilevers when irradiated with a laser beam.

A secondary objective of the initial modeling effort is to accurately calculate the peak temperature and temperature gradient in the cantilever when it is irradiated with the laser beam. Hence, very fine computational meshes are created across the thickness of this cantilever and around the region where the laser spot is located (Fig. 6). Computational meshes are also clustered together near the anchor of the cantilever where the stresses are likely to be the highest. On the contrary, the computational meshes near the tips of the cantilever are set relatively coarser because the stresses in that region are relatively smaller.

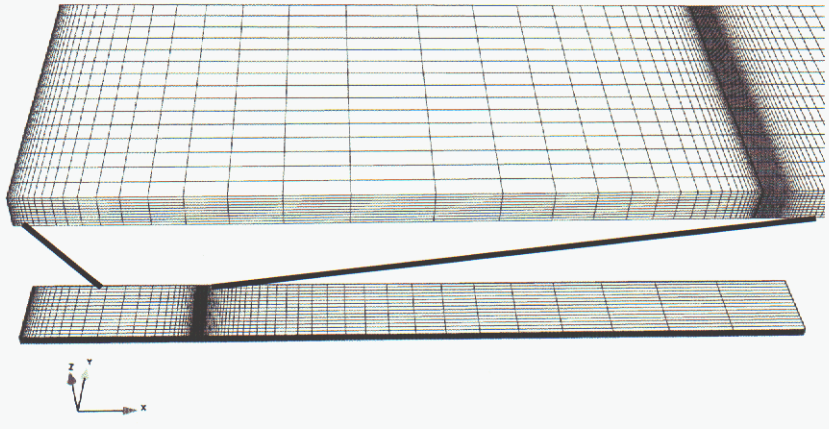

Fig. 6. Computational mesh system of the Neyoro-G™ cantilever.

When setting up Calagio to analyze the thermo-mechanical responses of a Neyoro-G™ cantilever, a few desired boundary conditions are imposed at a specific time so that the transient simulation follows closely with the testing procedure as in the experiment. For example; the tips of cantilever will be initially pushed downward to displace at a specific initial deflection. This is accomplished by imposing an internal force at the tip of the cantilever that creates an equivalent deflection as given in the experiment. Next, to model the optically heating from laser, a heat flux boundary condition is applied onto the top surface of the cantilever. The shape of the prescribed surface heat flux is elliptic with major axis of 2.2 mm and minor axis of 1.1 mm. In addition, this spatial heat flux profile is a quadratic function. It has a '$1/r^2$' dependency; where r is the distance between a node location of the computational mesh and the center of the elliptical laser spot. This optical heating model, written as a special user-subroutine, is then compiled, linked and incorporated onto the Calagio computer program. When the transient time reaches 20 ms, which corresponds to the duration of the laser pulse, the incident surface heat flux will be zero, implying that the laser beam has been turned off.

When setting up Calagio to analyze the thermo-mechanical responses of the Neyoro-G™ cantilevers, specific boundary conditions are imposed at specific time so that the transient simulation follows closely with the testing procedure. For example; the tips of cantilever will be initially pushed downward to displace at a desired initial deflection. This is accomplished by imposing internal forces at the tips that create an equivalent deflection as given in experiment. Next, to model the optically heating from laser, a heat flux boundary condition is applied onto the top surface of the cantilever. The shape of the prescribed surface heat flux is elliptic with major axis of 2.2 mm and minor axis of 1.1 mm. In addition, the heat flux profile has a '$1/r^2$' dependency; where r is the distance between a node location of the computational mesh and the center of the elliptical laser spot. This optical heating model, written as a special user-subroutine, is then compiled, linked and executed with the Calagio computer program. When the transient time reaches 20 ms, which corresponds to the duration of the laser pulse, the incident surface heat flux will be zero, implying that the laser has been turned off.

Similar to the experimental procedure, at the transient time of 40 ms, the applied internal force at the tip will be removed and the permanent deflection at the tip will be calculated and compared against the measurement. In these Calagio simulations, unlike in the experiment, the removal of the internal force at the tip is not instantaneous; there is a time-interval of 0.1 ms for the force to be totally removed. That is, a linear time decay function, instead of a step time function, is used to prescribe the change of the internal force as a function of time. This is done to prevent creating a stiff matrix when solving the governing equation in Calagio numerically. This setup allows Calagio to achieve a converged solution within a reasonable number of iterations.

2.2 Conical Forms

A circular piece of sheet metal, known as the cone pre-form, has been modeled and meshed for the FEA (Fig. 7). This circular metal substrate has a diameter of 6 mm and a thickness of 0.127 mm. In order to model the optical heating accurately and to minimize any numerical error, computational meshes are clustered around the annular region where the laser beam spot rotates about the center.

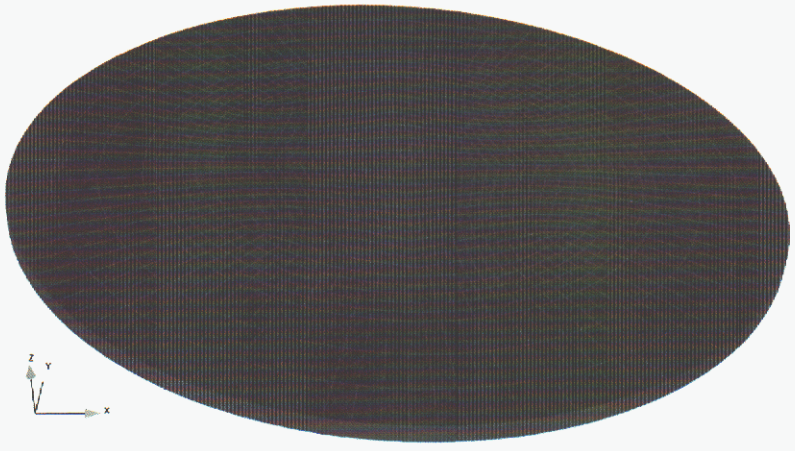

Fig. 7. Computational model used in the Calagio analysis of laser micro spinning.

The standard material properties for 304L stainless steal are used in this Calagio simulation. All the critical properties are temperature-dependent. One critical material property is the surface absorption coefficient. This determines how much the laser energy is absorbed or reflected. This property is very difficult to determine accurately due to its dependency on surface roughness and the presence of a thin film of foreign substance, such as an oxide layer.

The initial simulations had the parameters set up to match one of the preliminary experiments that had been completed (see section 3.2). The following laser parameters are used in the simulations, unless otherwise noted:

- Laser power: 8 W;
- Laser spot diameter: 0.04 cm;
- Speed of laser beam rotating around the disc: 0.71cm/s;
- Path diameter of laser beam: 0.35 cm.

In addition, the laser heating of the sheet metal is modeled as an applied surface heat flux boundary condition in these simulations. A special user-subroutine, "*qflux-moving.f*", is written, compiled, and linked with the Calagio program (see Appendix I).

3.0 Laser Micro Forming Experiments

The following sections describe the objectives and procedure for laser micro forming experiments. Two experimental programs were conducted. The first was micro forming of Neyoro-G™ contacts with pre-process applied deflection. The second is an experimental investigation of micro laser spinning of stainless steel conical forms.

3.1 Micro Forming of Contacts with Applied Deflection

The laser system used for the experimentation was a Lumonics (now GSI Group) JK702H Nd:YAG Laser with an adjustable pulse duration of 1-30 ms operating at 1064 nm fired in single shot mode. Each pulse is divided into temporal segments that can be individually changed in intensity. The entire pulse used here is 20 ms in duration, with the first millisecond programmed to be half the intensity of the rest of the pulse duration. This was done in order to correct an initial spike of intensity seen during pulse measurements to give a more uniform temporal intensity profile. The laser ran at a relatively steady 31 Watts, but the energy content per pulse would vary between 6 and 6.6 J per pulse.

The sample was suspended cantilever from its mount above a proximity sensor that has a 5 mm diameter (see Fig._. 8). The sensor's voltage output was calibrated by using the motion stages to move the sample up and down in relation to the sensor. The sensor has a linear response within 1 mm and a 2 μm resolution.. The elliptical laser spot (shaped by a -750 mm cylindrical lens and a 100 mm plano-convex lens) was focused such that the slow focal axis was at its minimum when it hit the samples, creating the most line-like focus. The focal spot was approximately 6 mm from the end of the sample in the mounting block and 12 mm from the end that was suspended over the proximity sensor. Assuming the sensor detects distance from its center, we calculate that the detected deflection point is 9.5 mm from the laser spot, which can be used to determine deflection angle. For the tip to move 25 μm at the distance of 12 mm from the laser spot, the bend angle is 2.1± 0.8 mrad. Because the sensor measures deflection at a distance of 9.5 mm from the focal line, that baseline should be used to calculate the deflection angle.

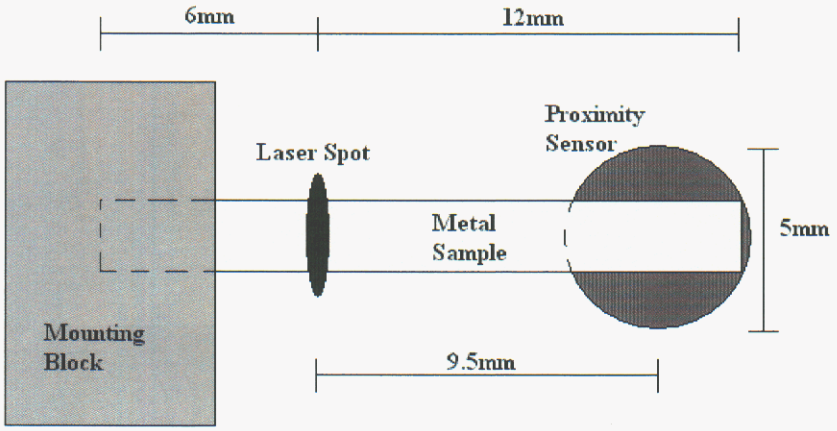

Fig. 8. Overhead view of laser bending setup.

A second measurement method was also used which compensated for the limited range of the inductance sensor (Fig. 9). A mechanical bar was suspended over the sample (Fig. 9) and attached to a digital slide micrometer. The micrometer could be positioned to a resolution of 10

micron increments using an attached manual translation stage with a high resolution micrometer screw. This bar had a dual purpose; it could also impose and maintain a mechanical stress on the sample during the laser bending process and measure the deflection amount after initial contact. For the testing, the proximity sensor is zeroed with the bar far away from the sample, since the metal of bar would interfere with the inductance based distance reading. The bar is then lowered down until it touches the sample. The continuity function on a multimeter was used to register contact between the bar and the sample. Contact was also confirmed visually. Once the contact was established, the micrometer was adjusted to bend the sample to the desired geometry. The laser was fired to induce the temperature gradient sufficient to bend the metal while the bar remains in contact. The bar was then removed from the object and lowered back down to test the new contact position with the sample. Then the bar was retracted far enough from the sample to prevent interference with the inductance sensor and the sensor reading was taken for a confirmation of the final position of the sample. At the higher deflection angles the inductance sensor had to be lowed away from the sample to avoid contact. This increased distance took the inductance sensor out of its linear operation region, so the micrometer was relied upon solely for those tests. When the inductance sensor was removed from the setup the metal bar could be used to induce upward and downward stresses and make the deflection measurements for both directions.

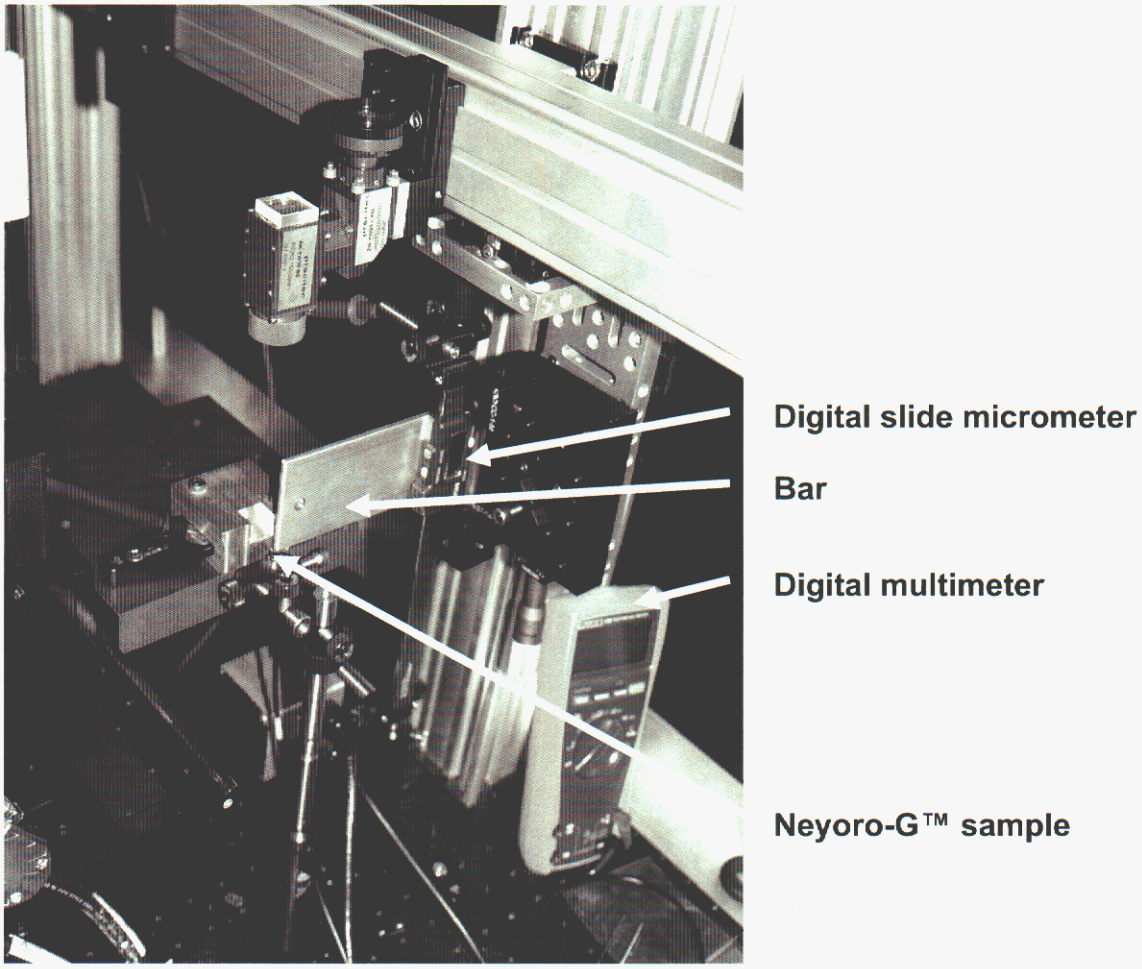

Fig. 9. Bending setup.

3.2 Laser Micro Spinning

Figure 10 depicts the apparatus for micro laser spinning of conical forms. The system

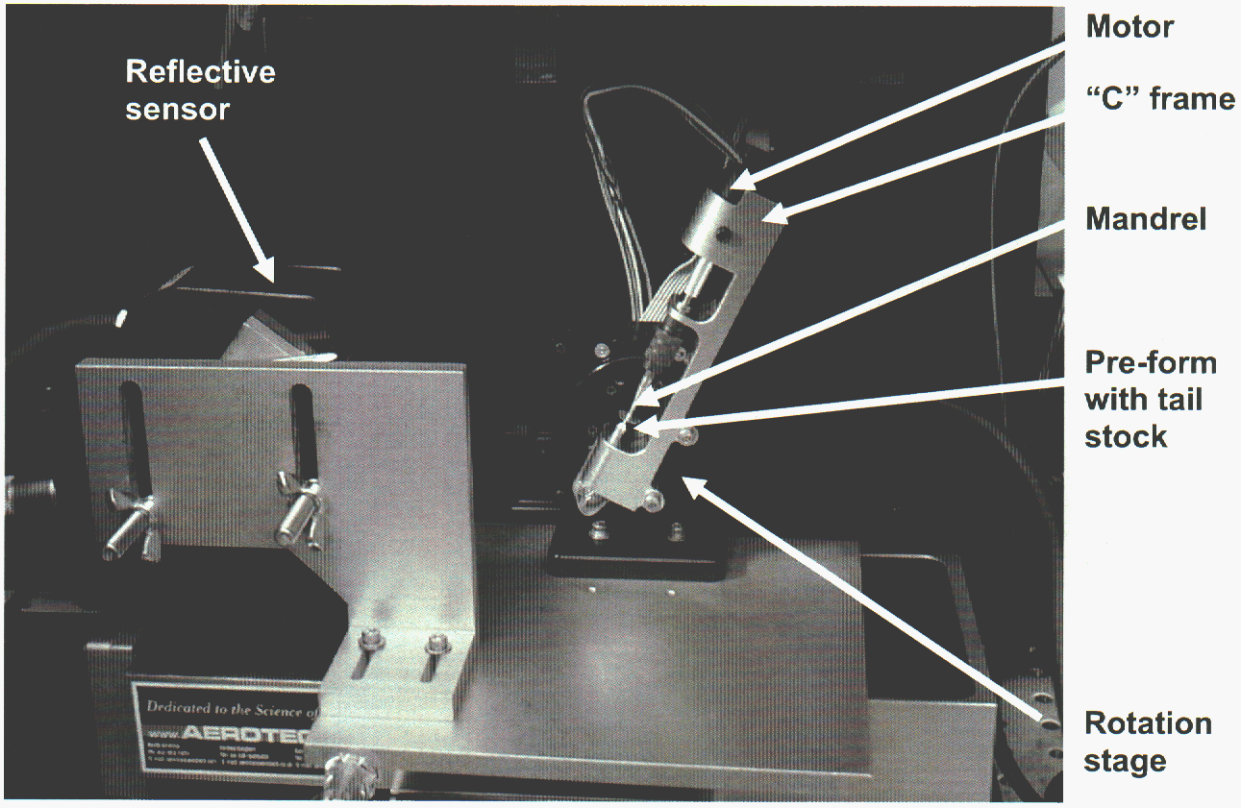

Fig. 10. Micro laser spinning apparatus.

consists of a "C" frame that houses an electric motor with speed control module (not shown). A copper mandrel is attached to the motor shaft. The 304L pre-form is fixed between the mandrel and spring-loaded tail stock assembly as shown. The motor rotates the pre-form at high angular velocity. Concurrently, a defocused 1064 nm laser beam is scanned (with a combination of beam scanning and "C" frame rotation) in a prescribed pattern on the upward-facing surface, thus initiating deflection. Deflection is measured by reflective sensor shown. In the ideal case, the applied centrifugal strain amplifies laser-induced deflection and causes the piece to form to the contour of the mandrel.

4.0 Results

4.1 Numerical Simulation: Micro Forming of Contacts

Results of the Calagio analyses of the thermo-mechanical responses of a Neyoro-G™ cantilever from laser heating are summarized in Table 4.1.1. The dimension of this cantilever is 9 mm long, 1.3 mm wide and 170 μm thick. Permanent deflections at the tip of this cantilever after being irradiated with a laser pulse of 5.5 joules for 20 ms have been calculated for five cases with different initial tip displacements.

Table 6. Comparison of Permanent Deflection Predicted by Calagio against Measurement

Initial Displacement	50 μm	100 μm	250 μm	500 μm	750 μm
Measured Permanent Deflection	5 μm	32 μm	30 μm	54 μm	81 μm
Calculated Permanent Deflection	0.538 μm	1.047 μm	2.563 μm	5.883 μm	31.63 μm

Fig. 11 plots the history of the calculated maximum temperature and vertical displacement. This plot illustrates the time sequence of events in the transient analysis to simulate the testing procedure. For example, the internal downward forces are initiated at the beginning of the transient and removed at 60 ms, and the laser power is turned on at 0.1 ms and off at 20.1 ms. Figure 12 shows the temperature distribution of the cantilever at 20 ms, when the laser power is just about being turned off. The high slope of the spatial temperature profile reveals that a fine computational mesh system is needed around the laser spot location and also across the thickness of the cantilever so that Calagio can calculate the peak temperature and temperature gradient accurately. Finally, for the case in which the initial displacement is 250 μm, Fig. 13 plots the permanent downward deflection profile along the cantilever after being irradiated with the laser beam of 5.5 joules for 20 ms.

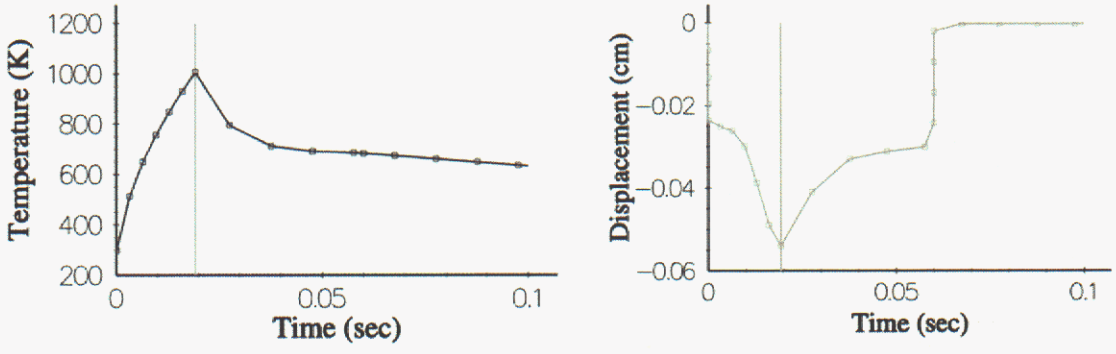

(a) (b)

Fig. 11. (a) History of the calculated maximum temperature and, (b) Downward displacement for the case in which the initial displacement is 250 μm.

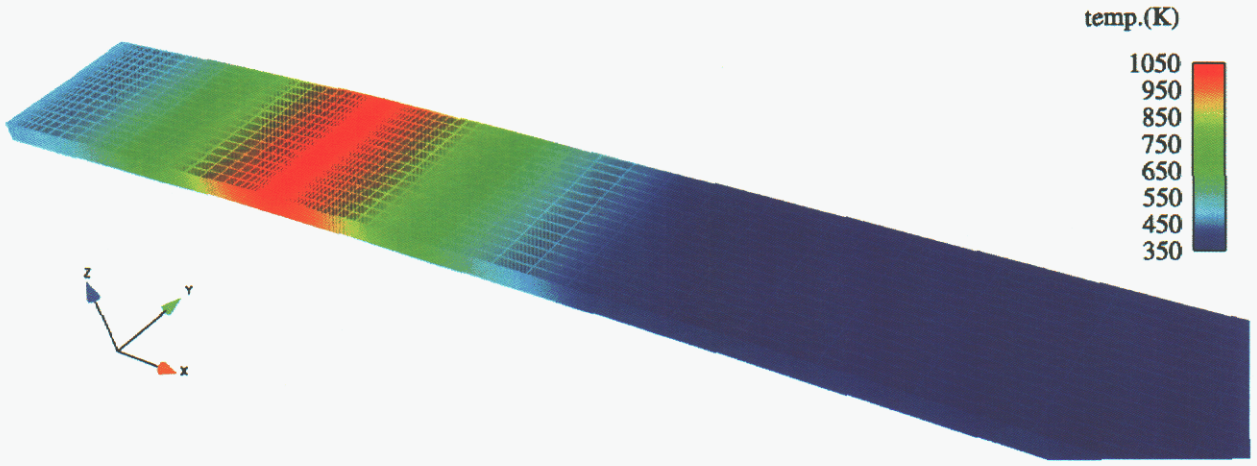

Fig. 12. Temperature profile of the Neyoro-G™ cantilever calculated by Calagio at 20 ms just before the laser beam is turned off.

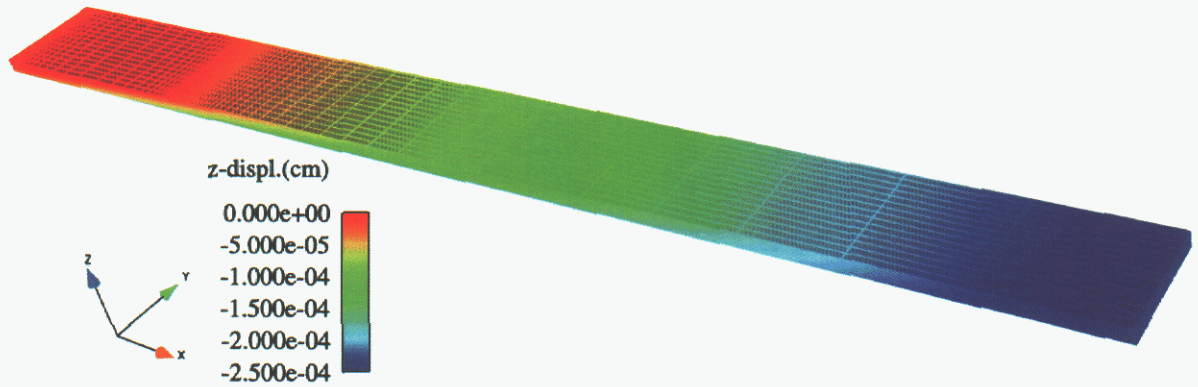

Fig. 13. Vertical displacement along the Neyoro-G™ cantilever calculated by Calagio at 0.1 sec.; the initial displacement is 250 μm downward.

Overall the calculated permanent deflection compares reasonably well with the experimental measurement, though some discrepancy exists between prediction and measurement. Nevertheless, these results are very encouraging, considering that moderate uncertainties do exist in the physics and engineering models in Calagio and also in the repeatability and accuracy of the measurement (Section 4.3). For example in optical modeling, the optical-to-thermal energy conversion rate is not well quantified as a function of temperature. Other material properties such as the yield stress are not well characterized at the elevated temperature above 1000 K. To evaluate the effect of these uncertainties on the permanent deflection, a sensitivity study has been performed. Result of the study will be discussed in the following segment.

The focus of this sensitivity study is to address the effect of varying different optical and heat transfer parameters on the permanent deflection of the cantilever. The first parameter of interest is the optical-to-thermal energy conversion rate or the laser absorption rate. In previous Calagio analyses, a constant value of 0.65 is used. By increasing the absorption rate to 0.8, Calagio predicts that the cantilever will be hotter and this leads to a larger permanent deflection (see Table 7).

Table 7. Effect of Higher Absorption Rate on Maximum Temperature and Permanent Deflection

Absorption Rate	Maximum Temperature	Initial Displacement	Permanent Deflection
0.65	1024 K	250 μm	2.563 μm
0.80	1191 K	250 μm	9.126 μm

The second parameter of interest is the laser energy absorption profile, which is modeled as a surface heat flux boundary condition in the Calagio analyses. We vary the heat flux profile and evaluate its effect on the plastic deformation of the cantilever. For this sensitivity study, instead of imposing a quadratic profile, a flat surface heat flux is applied. New results show that only a small difference in maximum temperature and permanent deflection is predicted (2nd row in Table 8). However, if the spot size is reduced from 2.2 mm long to 1.35 mm long, the maximum temperature will increase significantly (3rd and 4th row in Table 4.1.3). Subsequently, a larger permanent deflection at the tip of cantilever, 33.73 μm versus 2.56 μm, is calculated.

Table 8. Effect of Laser Profile on Maximum Temperature and Permanent Deflection

Flux Profile	Spot Size	Maximum Temperature	Initial Displacement	Permanent Deflection
Quadratic	1.1 mm * 2.2 mm	1024 K	250 μm	2.56 μm
Flat	1.1 mm * 2.2 mm	1034 K	250 μm	3.97 μm
Quadratic	1.0 mm * 1.35 mm	1441 K	250 μm	26.09 μm
Flat	1.0 mm * 1.35 mm	1504 K	250 μm	33.73 μm

It is mentioned in Section 3.1 that the energy content per laser pulse can vary between 5.5 and 6.6 joules per pulse. Hence a sensitivity study was performed to determine how the cantilever will respond to an increase in the laser energy per pulse. Table 9 shows how much the calculated maximum temperature and permanent deflection will change if the laser energy per pulse is increased from 5.5 joules to 6 joules and 6.6 joules, respectively.

Table 9. Effect of Laser Energy on Maximum Temperature and Permanent Deflection of Cantilever.

Laser Energy	Maximum Temperature	Initial Displacement	Permanent Deflection
5.5 J for 20 ms	1024 K	250 μm	2.56 μm
6 J for 20 ms	1090 K	250 μm	4.11 μm
6.6 J for 20 ms	1169 K	250 μm	7.90 μm

Amongst these Calagio analyses, the heat losses to the surrounding air and structures is considered to be relatively small. The heat transfer coefficient which models the convective heat losses is set to be 0.003 W/cm^2 K. Using this value implies that the laser micro forming process is performed in the ambient environment and the only convective heat loss is via natural convection[16]. Besides convection, radiation heat loss is also included in these Calagio analyses. Further analysis indicates that the effect of radiation loss on permanent deflection is relatively small (Table 10). However, if the micro forming process is conducted in a well-vented environment, the surrounding air is probably moving due to a venting fan being turned on. Air motion will induce more forced convective cooling and will affect the outcome of the micro forming process. The maximum temperature and permanent deflection will likely be much smaller, depending on the velocity of the moving air generated by the venting fan.

Table 10. Effect of Heat Loss to Surrounding Air and Structures on Maximum Temperature and Permanent Deflection

Radiation Loss	Convective Heat Transfer Coefficient	Maximum Temperature	Initial Displacement	Permanent Deflection
yes	0.003 W/cm^{2}K	1024 K	250 μm	2.56 μm
no	0.003 W/cm^{2}K	1025 K	250 μm	2.62 μm
yes	0.05 W/cm^2 K	1009 K	250 μm	1.38 μm
yes	1.0 W/cm^2 K	788 K	250 μm	0.014 μm

Laser micro forming of a Neyoro-G™ cantilever (9 mm long, 1.3 mm wide, and 170 micrometers thick), which is clamped at its base, has been simulated using the coupled physics code, Calagio. Reasonably good comparison between the calculated and measured permanent deflection has been obtained. Calagio result demonstrates that it can be applied to model the plastic strains induced by heating from a single laser pulse, followed by conductive and convective cooling. Various laser micro forming process parameters such as optical absorption rate, beam profile, spot size have been evaluated. More results from additional parametric studies will be presented in Appendix II. These simulation results will help establishing the basic process parameters for micro forming displacements with the desired 25-micrometer magnitude. However, more high-quality experimental work is still needed to validate the optical, thermal, and mechanical models and to reduce the uncertainty in material properties and physics models in Calagio.

4.2 Numerical Simulation: Conical Forms

This section presents the Calagio prediction of the thermal and mechanical responses of a circular sheet metal when irradiated with a rotating laser beam. Temperature calculation will be compared against the measured data obtained from the thermal couples installed in the experiment. Fig. 14 shows the calculated temperature profiles at time = 1.0 and 1.54 seconds, respectively. In this transient analysis, the peak heat flux location is set up to move counter-clockwise along an annular region, simulating the counter-clockwise rotation of the laser hot spot during the experiment. The thermally induced strain calculated by Calagio is plotted in Fig. 15. The shape of the disc is distorted in the figure because the calculated displacement has been magnified hundreds of times to reflect the geometric changes in the disc due to the thermally induced plastic deformation.

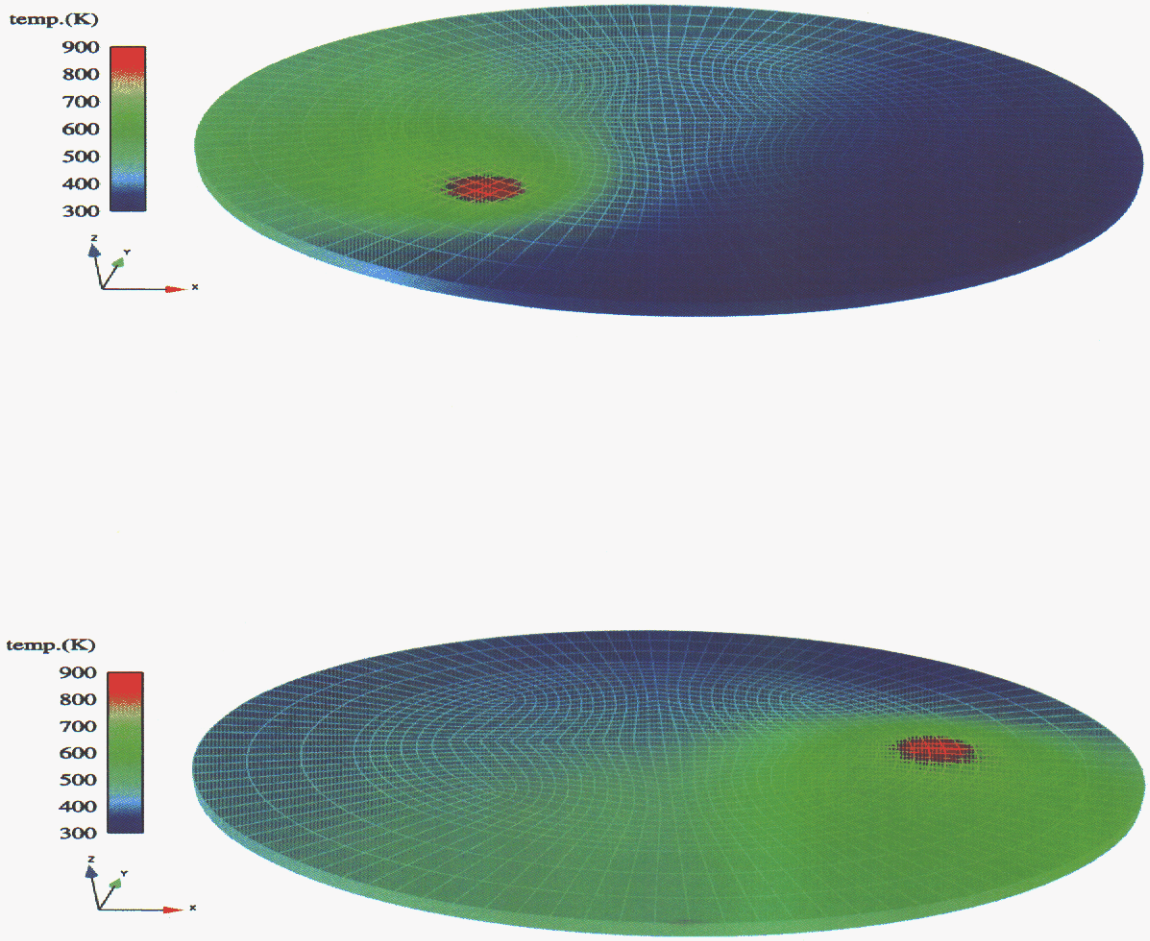

Fig. 14. Calculated temperature profiles at time = 1.0 second (top) and 1.54 seconds (bottom).

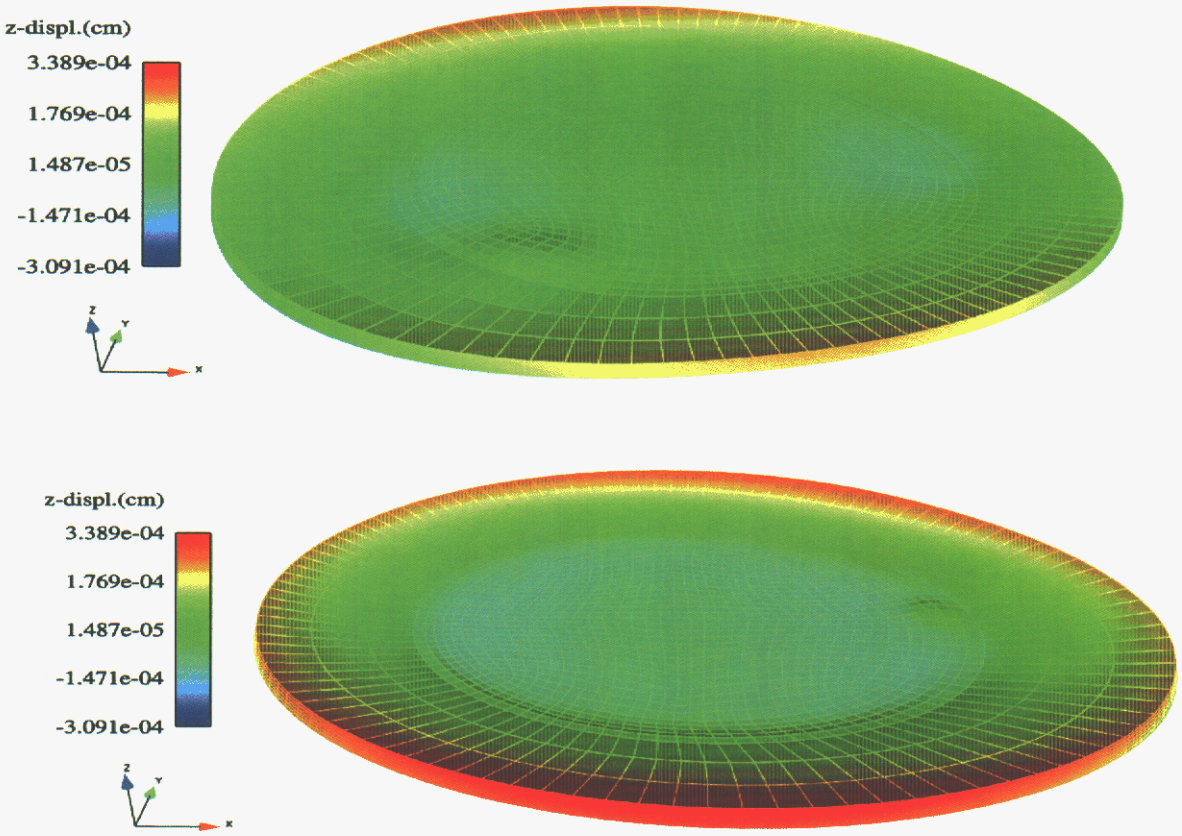

Fig. 15. Calculated thermally-induced strain at time = 1.0 sec. (top) and 1.54 sec. (bottom).

To assess the Calagio analysis and to validate its models, temperature history at a location is compared to experimental data under similar conditions. The location of interest corresponds to the location of a thermal couple (TC) installed in the experiment. Fig. 16 compares the calculated temperature against measurement from TC-1. The plot shows that the peak temperature is in good agreement. The predicted thermal response of the circular sheet metal does not cool off as quickly as observed in the experiment. In addition, Calagio fails to capture the second peak of the temperature history curve, which has a lower magnitude than the first peak. The temperature comparison between prediction and measurement obtained from TC-3 also shows good agreement with the peak temperature. The magnitude the second peak is over estimated by about 100 °C. The same discrepancy in cooling can also been applied, as in the previous plot. This has to do with the difficulties in determining the convective heat transfer coefficient accurately. Additional information about the environment conditions during the testing is needed to better formulate the convective heat transfer coefficient. The present calculations use a constant value of 0.01 W/cm^2 K. More work is needed to characterize the convective heat loss and to determine a more reliable and accurate heat transfer coefficient.

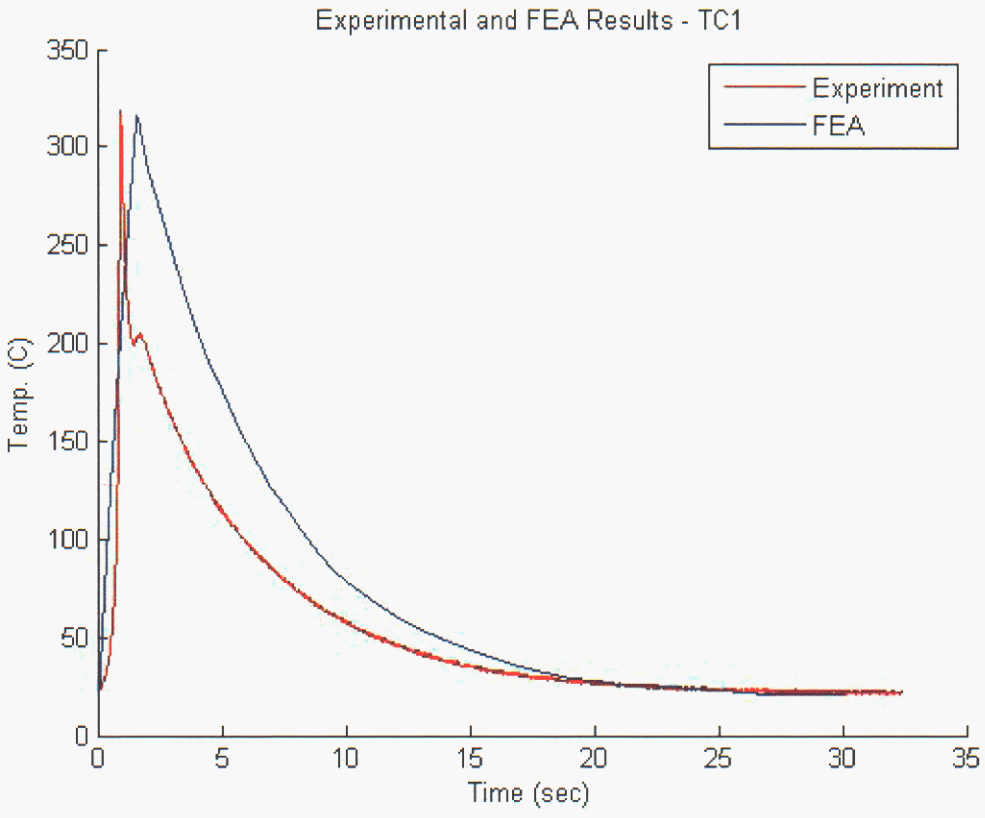

Fig. 16. Temperature history showing the comparison between prediction and TC-1.

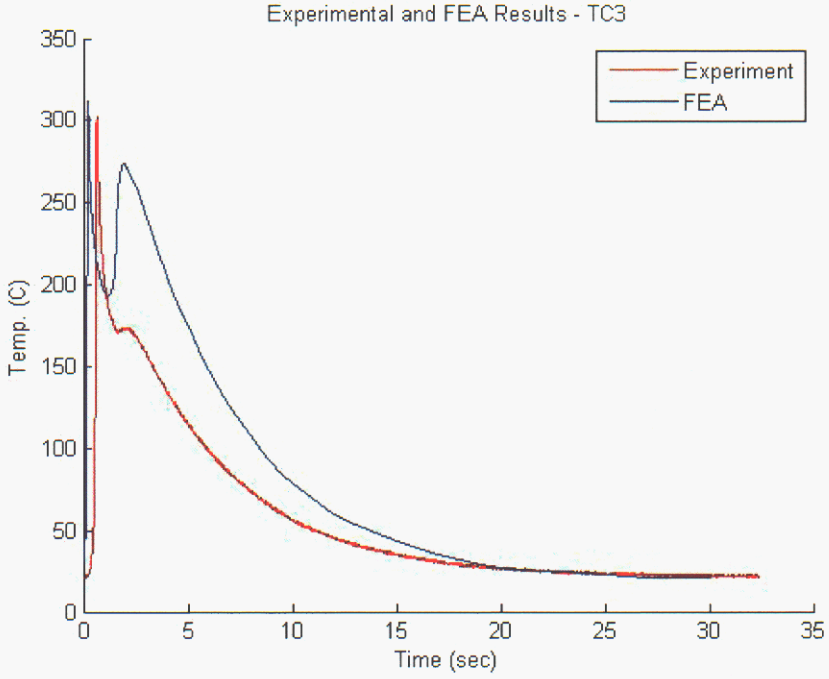

Fig. 17. Temperature history showing the comparison between prediction and TC-3.

For any permanent deflection to occur, the induced thermal stain must cause plastic deformation. Fig. 18 shows the equivalent plastic strain at the end of a simulation. The plastically strained region, represented by green area, is almost entirely limited to the same area the laser beam traversed.

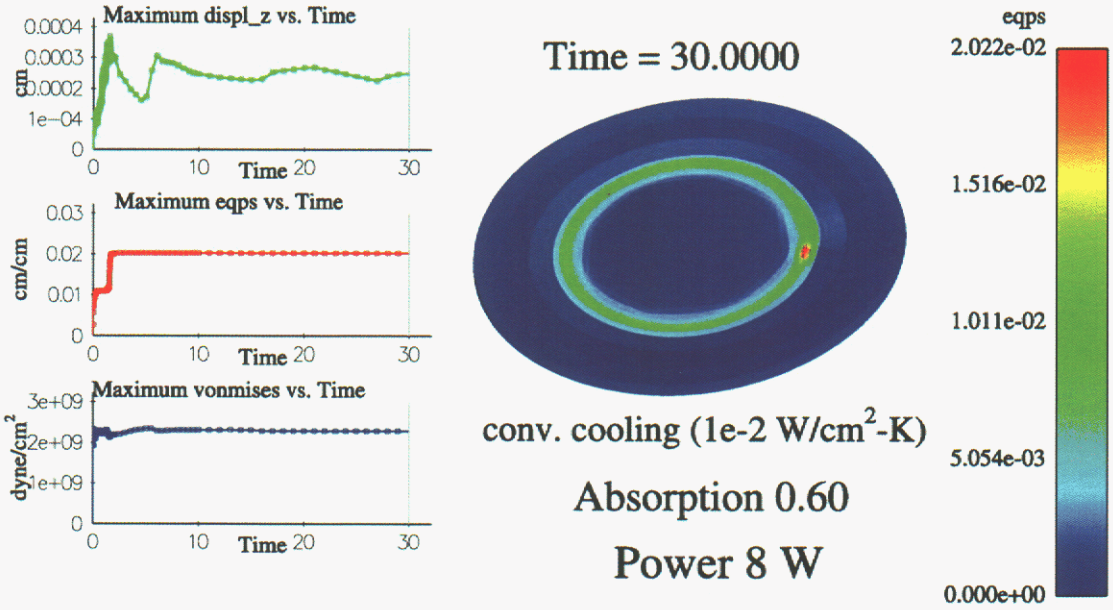

Fig. 18. Plot of the equivalent plastic strain predicted by Calagio.

4.3 Experiment: Micro Forming of Contacts

An initial test was conducted to verify the direction and magnitude of bending when there is a pre-stress in the upward or downward direction. The pulse energy for testing ranged between 6 and 6.6 J/pulse with random fluctuations of the laser system, but a power of 31 Watts was maintained. Below this energy level the pulse had little to no effect on the material surface and did not result in bending. Three tests were done in each direction at three different pre-applied deflection distances. Only three trials were run to investigate trends, and that number of repetitions was insufficient to draw conclusions with statistical confidence. Table 111 displays the resulting bends at the different pre-applied deflection conditions. The tests showed that all of the final positions are in the direction of the pre-applied displacement between 1 and 3mm in both directions. Note the pre-applied deflection in the upward direction resulted in a much smaller degree of overall bend.

Table 11. Loading of A Sample During Laser Forming,
(Negative Denotes Downward Bend, And Positive Is Upward)

6J, 20ms pulse, single shot			
Downward load		Upward load	
Distance (mm)	Final position (mm)	Distance (mm)	Final position (mm)
-1	-0.11	1	+0.09
-1	-0.15	1	+0.07
-1	-0.17	1	+0.08
-2	-0.48	2	+0.36
-2	-0.89	2	+0.30
-2	-0.83	2	+0.32
-3	-2.00	3	+0.79
-3	-1.60	3	+0.63
-3	-1.97	3	+0.61

After the directional deflections were examined, a more targeted test was performed to get statistical information on the resultant bend after stresses of varying degrees. The micro forming experiments were conducted with an applied deflection of 50, 100, 250, 500, and 750 microns, 15 trials of each. The results are shown in Fig. as a box and whisker plot representing the median, 1st and 3rd quartiles, endpoints, and outlier which are found outside these quartiles, beyond 1.5 times the inter-quartile range. The mean, median, and standard deviation of the 15 trials for each of the five stressed bending situations is shown in Table 12. From the median values it is apparent that increasing the amount of stress in the sample increased the final deflection of the samples progressively. The mean showed a similar trend except the outliers for the 100 micron bend skewed the mean and standard deviation high, but had little effect on the median. As stress increased, the variability tended to increase as well. The largest deflection had a wide range of resultant bend angles, but no final bend distance ever exceeded the displacement applied to it.

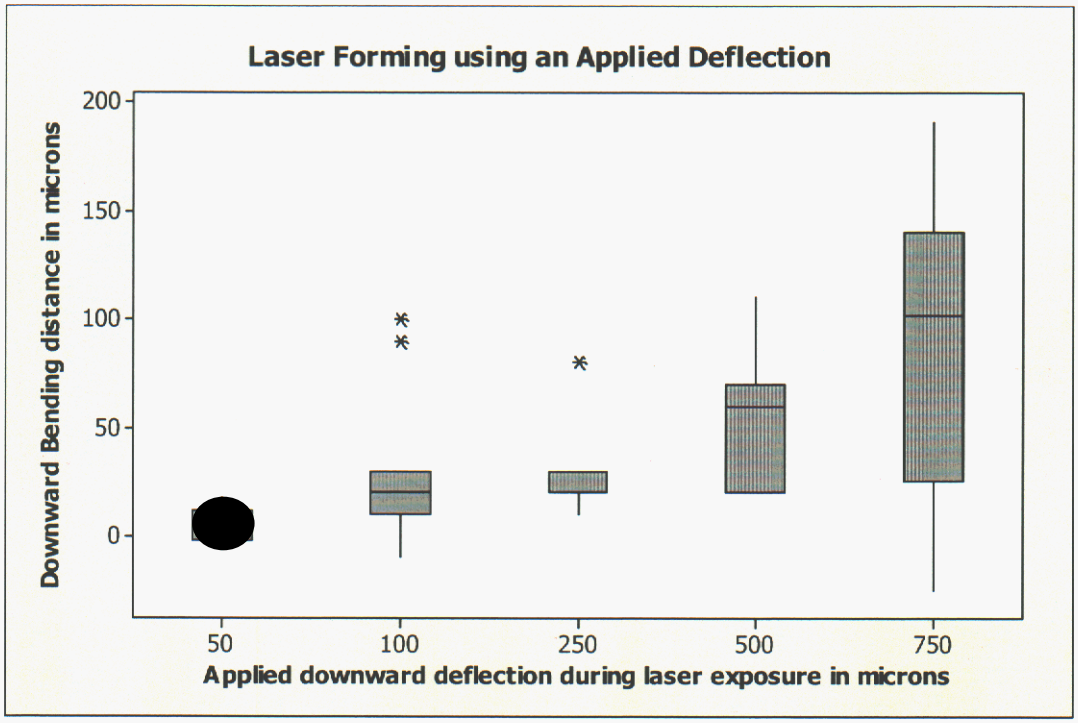

Fig. 19. Box plot of final deflection of 5 various lengths with 15 data points each.

Table 12. Resultant Bend Deflection Statistics Over 15 Trials at Five Different Stressed Positions

Bend distance statistics for 15 trials			
Downward Stress (microns)	Mean (microns)	Median (microns)	St. Dev. (microns)
50	5	4	7
100	32	20	34
250	30	30	13
500	54	60	32
750	81	102	67

Examining the spots made on the samples by the laser showed that there was large variability to the amount of discoloration made on the sample. Some laser spots would just appear as small darkened areas, while others were larger and had a light colored melt regions on the surface near the center. Based on visual inspection, larger deflections resulted from larger apparent spot sizes. The laser itself fluctuated in energy per pulse, as noted earlier, which could account for some of the randomness in the data.

The resolution of the micrometer used for measurements was 10 μm, and the inductance sensor could measure down to 2 μm in its linear range. The data for 50 and 100-μm deflections were taken from the inductance sensor and the other data for the larger deflection distances was drawn from the micrometer (due to the nonlinear response of the inductance sensor at those larger distances). The micrometer had the added error of manual adjustments and readings. The user had to watch the contact between the bar and sample while listening for the continuity circuit to trigger. The bar was lowered by hand and contact could be established within 20 microns (±10). Thus, regarding the difference of initial and final reading, the error was 28.3, or (rounded of to the significant figures of the measurement of the micrometer) 30 μm.

4.4 Laser Micro Spinning

At publication time, the laser micro spinning apparatus was assembled. In a preliminary operational (non-optical) test, the apparatus was run with a part in place (adhesively bonded to the tailstock; not soldered as is intended in the final use). Results of the operational tests revealed sensitivity in the final length of the retaining tailstock spring: If the spring was too short, the tailstock did not properly engage the sample. Conversely, the longer spring applied a high load on the motor, leading to stalling. As assembled, the sample initially rotated as designed with an acceptable level of lateral vibration. Shortly thereafter, the sample tended to "walk" off the tailstock. Adjustments to the spring length, the coupler/collet combination, and the tailstock are recommended to improve constraint of the sample.

5.0 Conclusions and Future Work

This project advanced laser micro forming of small, thin precious metal substrates and meso scale conical forms. The laser micro forming capability is the basis for a future disruptive meso manufacturing system that may include large deflection of metallic links, laser welding, and laser machining that enables component assembly without fasteners or human intervention.

Single-pulse laser micro forming of a Neyoro-G™ cantilever was simulated using the coupled physics code, Calagio. Reasonable agreement was obtained in several cases. Results demonstrate that it can be applied to model the plastic strains induced by heating from a single laser pulse, followed by conductive and convective cooling. Sensitivity studies were conducted for selected process parameters such as optical absorption rate, beam profile, and spot size. A reduction in laser spot size was determined to have the greatest effect on permanent deflection in the system. Additional experimental work is necessary to validate the optical, thermal, and mechanical models and to reduce the uncertainty in material properties and physics models in Calagio.

Laser micro forming was demonstrated for the first time as an alternative to manual manipulation in gap adjustment of Neyoro-G™ electrical contacts. A prescribed micro forming vector was achieved in single pulse irradiation of a Neyoro-G™ strip with cantilever end constraint and pre-applied tip deflection. Test results validated Calagio model data. In addition, the pre-applied displacement caused the sense of the micro forming vector to be deterministic in all cases. Note the pre-applied deflection in the upward direction resulted in a much smaller magnitude of the micro forming vector. Furthermore, the magnitude of the micro forming vector was found to be directly proportional to the magnitude of the pre-applied deflection. This research has validated the use of pre-applied deflection as a practical means of creating reproducible laser micro forming for electrical contact gap adjustment.

The concept of laser micro spinning was introduced. A Calagio model predicted the thermal and mechanical responses of a circular sheet metal when irradiated with a rotating laser beam. Temperature calculations were compared to measured data. The data shows good agreement with the peak temperature with discrepancies in other regions. Additional information about the environmental conditions during the testing is needed to better formulate the convective heat transfer coefficient and improve agreement. Future work will utilize the temperature distribution model to predict forming vectors in laser micro spinning of miniature conical forms.

References

1. H. D. Gilbert, *Miniaturization*, Reinhold Publishing Corporation, New York, 1961.
2. S. Kang, S. J., Lee, and F. B. Prinz, "Size does matter: The pros and cons of miniaturization," *ABB Review*, no. 2, pp. 54-62, ABB Asea Brown Boveri, Switzerland, 2001.
3. J. Magee, K. G. Watkins, and W. M. Steen, "Advances in Laser Forming," *Journal of Laser Applications,* vol. 10, no. 6, pp. 235-246, 1998.
4. F. Vollertsen, Z. Hu, H. Schulze Neihoff, and C. Theiler, "State of the art in micro forming and investigations into micro deep drawing," *Journal of Materials Processing Technology*, vol. 151, pp. 70-79, 2004.
5. M. Schmidt, M. Dirscherl, M. Rank, and M. Zimmermann, "Laser Micro Adjustment: From New Basic Process Knowledge to the Application," *Proceedings of the 2005 International Congress on Applications of Lasers and Electro-Optics (ICALEO 2005)*, pp. 96-105, 2005.
6. W. Hoving, "Opportunities and challenges for laser technology in microelectronics and photonics," *Proceedings SPIE*, vol. 4977, pp. 448-457, 2003.
7. M. Dirscherl, G. Esser, and M. Schmidt, "Ultrashort Pulse Laser Bending," *Journal of Laser Micro/Nano Engineering*, vol. 1, no. 1, pp. 54-60, 2006.
8. F. Vollertsen, "An Analytical Model for Laser Bending," *Lasers in Engineering*, vol. 2, pp. 261-276, 1994.
9. F. Vollertsen, I. Komel, and F. Kals, "The laser bending of steel foils for microparts by the buckling mechanism- a model," *Journal of Modeling and Simulation in Materials Science and Engineering*, vol. 3, pp. 107-119, 1995.
10. C. L. Yau, K. C. Chan, and W. B. Lee, "A New Analytical Model for Laser Bending," *Proceedings of LANE'97, Laser Assisted Net Shape Engineering,* vol. 2, pp. 357-366, 1997.
11. P. Cheng *et al.*, "Laser Forming of Varying Thickness Plate-Part I: Process Analysis," *Journal of Manufacturing Science and Engineering*, vol. 128, pp. 634-641, 2006.
12. D. F. Walczyk and S. Vittal, "Laser Forming of Titanium Aircraft Parts," *Transactions of NAMRI/SME*, vol. 29, pp. 111-118, 2001.
13. K. C. Lee and J. Lin, "Transient deformation of thin metal sheets during pulsed laser forming," *Journal of Optics and Laser Technology*, vol. 34, pp. 639-648, 2002.
14. G. Yanjin, S. Sheng, Z. Guoqun, and L. Yiguo, "Finite element modeling of laser bending of pre loaded sheet metals," *Journal of Materials Processing Technology*, vol. 142, pp. 400-407, 2003.
15. G. Dearden and S. P. Edwardson, "Some recent developments in two- and three-dimensional laser forming for 'macro' and 'micro' applications," *Journal of Optics: Pure and Applied Optics*, vol. 5, pp. S8-S15, 2003.
16. G. Yanjin, S. Sheng, Z. Guoqun, and L. Yiguo, "Influence of material properties on the laser-forming process of sheet metals," *Journal of Materials Processing Technology*, vol. 167, pp. 124-131, 2005.
17. Deringer-Ney, Inc., http://www.deringerney.com, 2006.
18. T. Lehecka, B. R. Campbell, and R. Campbell, "Laser Micro Forming of Contacts with Applied Deflection," 2006, unpublished.
19. T. Hennige, "Development of Irradiation Strategies for 3D-Laser Forming," *Journal of Materials Processing Technology*, vol. 103, pp. 102-108, 2000.
20. G. Casalino, and A. D. Ludovico, "Optimization and Modeling of Laser Forming of Stainless Steal Circular Sections," *Journal of Laser Applications*, vol. 15, pp. 85-95, 2003.

APPENDIX I: CALAGIO INPUT DECK & USER-SUBROUTINES

Micro Forming of Electrical Contact

Calagio Input

```
#:lineheat_aprepro.in
# Channy Wong (ccwong@sandia.gov)
# Bill Scherzinger(wmscher@sandia.gov)
# Frederick Livingston (fjlivin@sandia.gov) 07-25-2006

Begin sierra lineheat1
Title rectangular board / neyoro-G plane: \$
transient simulation; initially flat  \$
unit in cgs gm cm sec

 Begin Global Constants
  Stefan Boltzmann Constant = 5.67E-12
  Ideal Gas Constant = 0.287
 End

 ##########################################################################
 #                                        #
 # Defining Directions                              #
 #                                        #
 ##########################################################################
 define direction x with vector 1.0 0.0 0.0
 define direction y with vector 0.0 1.0 0.0
 define direction z with vector 0.0 0.0 1.0

 ##########################################################################
 #                                        #
 # Material Properties Functions                          #
 #                                        #
 # 1. thermal strain for Neyoro G needs to be found          #
 #   (Channy: use the constant from Jeremy Excel file;       #
 #          table is set up below.)                  #
 # 2. Young's modulus fundtion is known                  #
 # 3. Poisson's ratio is considered constant               #
 # 4. yield stress function is known                    #
 #                                        #
 ##########################################################################

 ## Youngs Modulus for a given Temperature
 begin definition for function youngs
  type is piecewise linear
  begin values
```

```
   293.0   1.00
   373.0   1.00
   473.0   0.95
   573.0   0.88
   673.0   0.70
   773.0   0.33
   873.0   0.17
  end values
end definition for function youngs

## Poissons Ratio for a given Temperature
begin definition for function poissons
  type is piecewise linear
  begin values
   293.0   1.00
   973.0   1.00
  end values
end definition for function poissons

##  Yield Stress for a given Temperature
begin definition for function yield
  type is piecewise linear
  begin values
   293.0   1.00
   373.0   1.56
   473.0   1.46
   573.0   1.08
   673.0   0.60
   773.0   0.21
   873.0   0.08
  end values
end definition for function yield



#########################################################################
#                                       #
# Thermal Properties Functions                    #
#                                       #
#########################################################################

## Thermal Strain for a given Temperature
begin definition for function THERMAL_STRAIN
  type is piecewise linear
  ordinate is strain
  abscissa is temperature
```

```
  begin values
    0.0    0.0
    1.0    1.2600e-5
   10.0    1.2600e-4
  100.0    1.2600e-3
 1000.0    1.2600e-2
10000.0    1.2600e-1
  end values
end definition for function THERMAL_STRAIN

## Initial Force acting on cantilever to case initial displacement
## Tip Deflected from 0.0001 seconds until the part cools
## -167.9938519 dyne force results in an -0.05mm displacement
## -335.9763584 dyne force results in an -0.10mm displacement
## -839.9973597 dyne force results in an -0.25mm displacement
## -1680.933760 dyne force results in an -0.50mm displacement
## -2524.192977 dyne force results in an -0.75mm displacement
## -3371.178249 dyne force results in an -1.00mm displacement
## -6825.901466 dyne force results in an -2.00mm displacement
## -10466.08174 dyne force results in an -3.00mm displacement

begin definition for function prescribed_f1
  type is piecewise linear
  begin values
            0.0000    0.0000
            0.00009  -839.9973597  # Apply Force to Tip and Hold there until it cools
    0.0600  -839.9973597
    0.0601   0.0
    1.0000   0.0
  end  values
end definition for function prescribed_f1

# Temperauture is reasonable without convective cooling
#  begin definition for function CONVECT_HTC
#    type is piecewise linear
#    ordinate is heat-transfer-coefficient
#    abscissa is time
#    begin values
#              0.0000   0.0000
#              0.0001  1.0000
#              0.0201  1.0000      # Laser Turns off at this time
#              0.0202  500.00
#     1.0000  500.00
#    end values
#  end definition for function CONVECT_HTC
```

```
 begin property specification for material neyoro
  Density = 15.9                    # gm/cm3
  Specific Heat = 0.1298              # J/gm K
  Thermal Conductivity = 2.98       # W/cm K
  Emissivity = 0.64
  thermal strain function = THERMAL_STRAIN

#   begin parameters for model elastic
#     youngs modulus  = 1.1e12            # dyne/cm2
#     poissons ratio  = 0.44              # approximate value for gold
#   end parameters for model elastic

  ######################################################################
  #
  # thermoelastic-plastic power law hardening description
  # for Neyeoro G
  #

  begin parameters for model thermo_ep_power

   youngs modulus    = 1.1e12        # dyne/cm2 - Youngs modulus for gold
   poissons ratio    = 0.44          # nd - Poissons ratio for gold

   yield stress      = 5.50e9        # dyne/cm2 - Neyoro G data from 1824
   hardening constant = 3.35e9       # dyne/cm2 - Neyoro G data from 1824
   hardening exponent = 0.3          # nd - Neyoro G data from 1824
   luders strain     = 0.0           # nd - assume no Luders strain
   beta              = 1.0           # nd - assume isotropic hsrdening

   youngs modulus function = youngs    # Neyoro G data from 1824
   poissons ratio function = poissons  # Neyoro G data from 1824
   yield stress function   = yield     # Neyoro G data from 1824

  end parameters for model thermo_ep_power

  #
  ######################################################################

 end property specification for material neyoro

 ########################################################################
 #                                      #
 # Element Block Definitions                    #
 #                                      #
 ########################################################################
```

```
begin finite element model mesh_calagio
  Database Name = cantilever1.par
  Database Type = exodusII

  begin parameters for block block_1
    material neyoro
    # solid mechanics use model elastic
    solid mechanics use model thermo_ep_power
  end parameters for block block_1

end finite element model mesh_calagio

##########################################################################
#                                        #
# BEGIN SOLVER                                    #
#                                        #
##########################################################################

Begin AZTEC Equation Solver solve_temperature
  Solution Method = cg
  Preconditioning Method = jacobi
  Maximum Iterations  = 2000
  Residual Norm Tolerance = 1e-06
  Residual Norm Scaling = NONE

End

 begin feti equation solver feti
   maximum iterations = 500
   maximum orthogonalization = 1000
   preconditioning method = dirichlet
   residual norm tolerance = 10e-3
   corner algorithm = 3
   corner dimensionality = 3
   corner augmentation = none
   coarse solver = skyline
   local solver = sparse
   num local subdomains = 32
   # debug output level = 2
 end feti equation solver feti


##############################################################################
#                                          #
# CALAGIO Time Control                                #
#                                          #
```

```
##########################################################################
begin calagio procedure Acca_Procedure

begin time control

  ##########################################################################
  #                                                        #
  # block p1 = initial tip deflection                              #
  #          80 load steps                                 #
  #          Steps 0 -> 80                                 #
  ##########################################################################
  begin time stepping block p1
   start time = 0.0

   Begin Parameters for Calore Region calore
    time step =  1.25e-6                  # Time Step
    transient step type = fixed
    time integration rule = implicit
    Predictor Rule is  forward euler
   End Parameters for Calore Region calore

   begin parameters for adagio region adagio
    time increment = 1.25e-6                  # Step Increments
   end parameters for adagio region adagio
  end time stepping block p1

  ##########################################################################
  #                                                        #
  # block p2 = laser heating of strip                              #
  #          120 load steps                                #
  #          Steps 80 -> 200                               #
  ##########################################################################
  begin time stepping block p2
   start time = 0.0001
   begin Parameters for Calore Region calore
    time step = 1.6e-4
    transient step type = fixed
    time integration rule = implicit
    Predictor Rule is  forward euler
   end Parameters for Calore Region calore
   begin parameters for adagio region adagio
    time increment = 1.6e-4 #2.0e-4
   end parameters for adagio region adagio
  end time stepping block p2

  ##########################################################################
```

```
#                                                    #
# block p3 = cooling fo beam                                  #
#          80 load steps                                #
#          Steps 200 -> 280                               #
#####################################################################

begin time stepping block p3
  start time = 0.0201
  begin Parameters for Calore Region calore
    time step = 5e-4
    transient step type = fixed
    time integration rule = implicit
    Predictor Rule is  forward euler
  end Parameters for Calore Region calore
  begin parameters for adagio region adagio
    time increment = 5e-4
  end parameters for adagio region adagio
end time stepping block p3

#####################################################################
#                                                    #
# block p4 = unloading tip                                    #
#          80 load steps                                #
#          Steps 280 -> 360                               #
#####################################################################

begin time stepping block p4
  start time = 0.06
  begin Parameters for Calore Region calore
    time step = 1.25e-6
              transient step type = fixed
    time integration rule = implicit
    Predictor Rule is  forward euler
  end Parameters for Calore Region calore
  begin parameters for adagio region adagio
    time increment = 1.25e-6
  end parameters for adagio region adagio
end time stepping block p4

#####################################################################
#                                                    #
# block p5 = beam near room temp                              #
#          100 load steps                               #
#          Steps 360 -> 460                               #
#####################################################################
```

```
  begin time stepping block p5
   start time = 0.0601
   begin Parameters for Calore Region calore
    time step = 5.0e-4
              transient step type = fixed
    time integration rule = implicit
    Predictor Rule is  forward euler
   end Parameters for Calore Region calore
   begin parameters for adagio region adagio
    time increment = 5.0e-4
   end parameters for adagio region adagio
  end time stepping block p5

  termination time =  0.10              # Simulation End Time
end time control

coupling region order = calore_adagio
coupling direction = one_way


##########################################################################
#                                        #
# CALORE Region                                  #
#                                        #
##########################################################################
 Begin Calore Region calore

  Use Finite Element Model mesh_calagio Model Coordinates are model_coordinates
  Use Linear Solver solve_temperature

  Begin Initial condition ICblock_0
   temperature = 298.0
   add volume block_1
  End


  ###################################################################
  #                                      #
  # THERMAL Output                               #
  #                                      #
  ###################################################################
  Begin Results Output Label diffusion output
   Database Name is lineheat1_ht.e
   Nodal Variables = temperature as TEMP
   At Step 0, Increment = 20
  End
```

```
Begin Heat Flux Boundary Condition bc1
        Element Subroutine is fixed_q
  # Real Data x0 y0 a0 b0 pwr abs pwrON pwrOFF
        # x0: Laser spot center xaxis    [cm]
        # y0: Laser spot center yaxis    [cm]
        # a0: Ellptical Spot major axis  [cm]
        # b0: Ellptical Spot minor axis  [cm]
        # pwr: Total power input         [Watts]
        # abs: Absorption
        # pwrON: Laser power on time     [secs]
        # pwrOFF: Laser power off time   [secs]
        #Real Data  -0.45  0.0 0.02 0.675 275 0.65 0.0001 0.0201  #5.5J 20ms
  #Real Data  -0.425 0.0 0.09 0.135 275 0.65 0.0001 0.0201
  Real Data   -0.425 0.0 0.11 0.22  275 0.65 0.0001 0.0201  #Penn State
        Add surface surface_200
  Add surface surface_201
  Add surface surface_202
End


#########################################################################
#                                       #
# Thermal Boundary Condition                      #
# Anchor is fixed to Room Temp                     #
#                                       #
#########################################################################
#Begin temperature Boundary Condition fix-end
#  add surface surface_101
#  temperature = 298.0
#End

#########################################################################
#                                       #
# Thermal Boundary Condition                      #
# Convection Boundary Condition for Top surfaces and Free-End Side #
#                                       #
#########################################################################
Begin Convective Flux Boundary Condition on bc-top-end
        Add surface surface_102
  Add surface surface_200
  Add surface surface_201
        Add surface surface_202
# # Convective Coefficient Time Function = CONVECT_HTC
        Convective Coefficient is 0.003  #H [W/cm^2*k]
  Reference Temperature is 298.0
```

```
 Integrated flux output topflux
End

##########################################################################
#                                                                        #
# Thermal Boundary Condition                                             #
# Radiation Boundary Condition for Top surfaces                          #
#                                                                        #
##########################################################################
Begin Radiative Flux Boundary Condition on bc-rtop
 Add surface surface_200
 Add surface surface_201
 Add surface surface_202
 Reference Temperature is 298.0
 Radiation Form Factor = 1.0
End

##########################################################################
#                                                                        #
# Thermal Boundary Condition                                             #
# Convection Boundary Condition for Bottom surfaces                      #
#                                                                        #
##########################################################################
Begin Convective Flux Boundary Condition on bc-bottom
 Add surface surface_300
 Add surface surface_301
 Add surface surface_302
 # Convective Coefficient Time Function = CONVECT_HTC
 Convective Coefficient is 0.003  #1.0
 Reference Temperature is 298.0
 Integrated flux output bottomflux
End

##########################################################################
#                                                                        #
# Thermal Boundary Condition                                             #
# Radiation Boundary Condition for Bottom surfaces                       #
#                                                                        #
##########################################################################
Begin Radiative Flux Boundary Condition on bc-rbottom
 Add surface surface_300
 Add surface surface_301
 Add surface surface_302
 Reference Temperature is 298.0
 Radiation Form Factor = 1.0
End
```

```
  End Calore Region calore

 begin adagio region adagio
  use finite element model mesh_calagio
  options = thermalstrain


   ###################################################################
   #                                                 #
   # MECHANICAL Output                                       #
   #                                                 #
   ###################################################################
  begin Results Output output_adagio
   Database Name = lineheat1_me.e
   Database Type = exodusII
   At Step 0, Increment = 20
   nodal Variables = force_external as f_ext
   nodal Variables = force_internal as f_int
   nodal Variables = velocity as vel
   nodal Variables = displacement as displ
   nodal Variables = temperature as temp
   nodal Variables = reactions as react
   element Variables = rotated_stress as stress

            ###########################################################################
#
            #
            element Variables = von_mises as vonmises
            element Variables = MAT%thermo_ep_power(1) as eqps
            element Variables = MAT%thermo_ep_power(2) as radius
            #
            ###########################################################################
#

   global Variables = timestep as timestep
  end results output output_adagio

  ###################################################################
  #                                                 #
  # Mechanical Boundary Condition                           #
  # Anchor-End is fixed to in x,y,and z direction             #
  #                                                 #
  ###################################################################
  begin fixed displacement
   surface = surface_101
```

```
  components = x y z
end fixed displacement

##########################################################################
#                                                                        #
# Mechanical Boundary Condition                                          #
# Prescribe Function of Force is place on Free-End in z direction        #
#                                                                        #
##########################################################################
begin prescribed force
  node set = nodelist_113
  node set = nodelist_114
  component = z
  function = prescribed_f1
end prescribed force


##########################################################################
#                                                                        #
# Solver definition                                                      #
#                                                                        #
##########################################################################
Loadstep predictor using line search type secant

   ################################################
   #  Predictor Scale Factor - Bill 08-01-2006  #
            predictor scale factor = 1.00 during period p1
            predictor scale factor = 0.00 during period p2
   predictor scale factor = 0.00 during period p3
   predictor scale factor = 1.00 during period p4
            predictor scale factor = 0.00 during period p5

  Begin adagio solver CG
    Target Residual              = 10.0e-3
    Target relative Residual     = 1.0e-3
    Maximum Iterations           = 50000
    Orthogonality measure for reset = 0.1
    Line Search type secant

    begin full tangent preconditioner
       linear solver = feti
       reset constraint threshold = 0.0
       nodal preconditioner method = elastic
       Balance probe = 1
    end full tangent preconditioner
```

```
    end   adagio solver CG

  end adagio region adagio
  end calagio procedure Acca_Procedure

  User Subroutine File is qflux-elp.f

end sierra lineheat1
```

Subroutine qflux-elp.f

```
      SUBROUTINE FIXED_Q ( FACEID, NELEMF, NINT, COORDS, T,
     &                     FLUX, IERROR )
      INTEGER FACEID, NELEMF, NINT, IERROR
      DOUBLE PRECISION COORDS, T, FLUX, RDAT(8)
      DOUBLE PRECISION TIME
      DOUBLE PRECISION pi, x0, y0, a0, b0, pwrmx, abp, qmx,
     &  time1, time2, x1, y1, xx, yy, rx2, ry2
      DIMENSION FACEID(NELEMF)
      DIMENSION COORDS(3, NELEMF, NINT)
      DIMENSION T(NELEMF, NINT)
      DIMENSION FLUX(NELEMF, NINT)
C*************************************************************
C Set the heat flux on the surface as a function of the
C surface coordinate, using real data parsed from the
C input file.
C*************************************************************
      INTEGER INTPT, FACE

C*************************************************************
      CALL ACAL_GET_INSTANCE_REAL_DATA( 8, RDAT )
      CALL ACAL_GET_TIME(TIME)

        pi = 3.14159265

c  center of the laser spot
        x0 = RDAT(1)
        y0 = RDAT(2)

c  1/2 of the major and minor axis of the ellptical spot
        a0 = RDAT(3)
        b0 = RDAT(4)

C  TOTAL POWER INPUT:
        pwrmx = rdat(5)
```

```
C  absorption
       abp = rdat(6)

       qmx = pwrmx*abp*24 / (pi*a0*b0*17)

c  set time interval for power to turn on
       time1 = rdat(7)
       time2 = rdat(8)

      if (TIME .ge. time1 .and. TIME .le. time2) then

       DO 20 INTPT=1,NINT
        DO 10 FACE=1,NELEMF
c         FLUX(FACE,INTPT) = 0.0
         x1 = COORDS(1,FACE,INTPT)
         y1 = COORDS(2,FACE,INTPT)
                  xx = (x1 - x0) / a0
                  yy = (y1 - y0) / b0
                  rx2 = xx**2
                  ry2 = yy**2
         IF (rx2 .le. 1.0 .and. ry2 .le. 1.0) then
           FLUX(FACE,INTPT) = qmx * (1-rx2) * (1-ry2)
                   ENDIF
   10    CONTINUE
   20   CONTINUE

      endif

      ERROR = 0
      RETURN
      END
```

Micro Conical Forms

Calagio Input

```
begin sierra cone pre-form test

Title rectangular board / 304L SS Cone Pre-form: \$
transient simulation; initially flat  \$
unit in cgs gm cm sec

 Begin Global Constants
  Stefan Boltzmann Constant = 5.67E-12
```

```
 Ideal Gas Constant = 0.287
End

##########################################################################
#                                                                        #
# Directions                                                             #
#                                                                        #
##########################################################################

define direction x with vector 1.0 0.0 0.0
define direction y with vector 0.0 1.0 0.0
define direction z with vector 0.0 0.0 1.0

##########################################################################
#                                                                        #
# Function Definitions                                                   #
#                                                                        #
##########################################################################

#
# Material Properties
#
# 1. thermal strain for 304L can be refined
# 2. Young's modulus function is known
# 3. Poisson's ratio is considered constant
# 4. yield stress function is known
#

begin definition for function thermal_strain
 type is piecewise linear
 begin values
    0.00   0.0000000
 1273.00   0.0226594
 end values
end definition for function thermal_strain

begin definition for function youngs
 type is piecewise linear
 begin values
   293.0   1.00
   311.0   1.00
   421.0   1.00
   533.0   0.96
   644.0   0.89
   755.0   0.86
   866.0   0.79
```

```
    977.0   0.71
   1089.0   0.64
  end values
end definition for function youngs

begin definition for function poissons
  type is piecewise linear
  begin values
    293.0   1.00
   1273.0   1.00
  end values
end definition for function poissons

begin definition for function yield
  type is piecewise linear
  begin values
     32.983333    1.2960
     88.538889    1.2660
    144.150000    1.2200
    199.705560    1.1520
    255.236670    1.0710
    293.000000    1.0000
    310.800000    0.9786
    367.094440    0.8624
    422.650000    0.7511
    477.483330    0.6790
    533.038890    0.6365
    589.316670    0.6250
    644.927780    0.6234
    699.761110    0.6217
    755.316670    0.6185
    810.872220    0.6070
    866.483330    0.5824
    922.038890    0.5464
    977.594440    0.4990
   1033.150000    0.4400
   1081.483300    0.3909
  end values
end definition for function yield

 begin definition for function therm_cond
  type is piecewise linear
  begin values
    273.0    0.162
    473.0    0.190
    673.0    0.214
```

```
   873.0    0.290
  1273.0    0.300
 end values
end definition for function therm_cond

 begin definition for function specific_heat
  type is piecewise linear
  begin values
    273.0    0.50
    473.0    0.54
    673.0    0.56
    873.0    0.59
   1273.0    0.61
  end values
end definition for function specific_heat

##########################################################################
#                                                                        #
# Material Model Definitions                                             #
#                                                                        #
##########################################################################

##########################################################################
#                                                                        #
# power law hardening model                                              #
#                                                                        #
##########################################################################

begin property specification for material SS_304L

  density         = 8.03                    # g/cm^3

  thermal strain function = thermal_strain      # cm/cm

  thermal conductivity function = therm_cond     # W/cm-K

  specific heat function = specific_heat    # J/g-K

  begin parameters for model ep_power_hard
    youngs modulus     = 193.e3              # MPa
    poissons ratio     = 0.30                #
    yield stress       = 227.0               # MPa
    hardening constant = 729.0               # MPa
    hardening exponent = 0.49                #
    luders strain      = 0.0                 #
  end parameters for model ep_power_hard
```

```
  begin parameters for model thermo_ep_power
    youngs modulus     = 193.0e10            # dyne/cm^2
    poissons ratio     = 0.30               #
    yield stress       = 227.0e07            # dyne/cm^2
    hardening constant = 729.0e07            # dyne/cm^2
    hardening exponent = 0.49               #
    luders strain      = 0.0                #
    beta               = 1.0                #
    youngs modulus function = youngs
    poissons ratio function = poissons
    yield stress function   = yield
  end parameters for model thermo_ep_power

end property specification for material SS_304L

###########################################################################
#                                                                         #
# Element Block Definitions                                               #
#                                                                         #
###########################################################################

begin solid section solid_1
  strain incrementation = strongly_objective
  use lame
end solid section solid_1

begin finite element model mesh1
  Database Name = cone_pre-form.g
  Database Type = exodusII

  begin parameters for block block_100
    material SS_304L
    solid mechanics use model thermo_ep_power
    section = solid_1
  end parameters for block block_100

end finite element model mesh1

###########################################################################
#                                                                         #
# BEGIN SOLVER                                                            #
#                                                                         #
###########################################################################

Begin AZTEC Equation Solver solve_temperature
```

```
  Solution Method = cg
  Preconditioning Method = jacobi
  Maximum Iterations  = 2000
  Residual Norm Tolerance = 1e-03
  Residual Norm Scaling = NONE
 End

 begin feti equation solver feti
  maximum iterations = 500
  maximum orthogonalization = 1000
  preconditioning method = dirichlet
  residual norm tolerance = 10e-3
  corner algorithm = 3
  corner dimensionality = 3
  corner augmentation = none
  coarse solver = skyline
  local solver = sparse
  num local subdomains = 32
#   debug output level = 2
 end feti equation solver feti

 ##########################################################################
 #                                        #
 # CALAGIO Procedure                              #
 #                                        #
 ##########################################################################

 begin calagio procedure Cal_Procedure

  ##########################################################################
  #                                        #
  # Time Step Definition                           #
  #                                        #
  ##########################################################################

  begin time control

    begin time stepping block p1
     start time =  0.0
     begin parameters for calore region calore
      time step = 0.005
      transient step type = fixed
      time integration rule = implicit
      Predictor Rule is  forward euler
     end parameters for calore region calore
```

```
    begin parameters for adagio region adagio
      time increment = 0.005
    end parameters for adagio region adagio
  end time stepping block p1

  begin time stepping block p2
    start time =  2.0
    begin parameters for calore region calore
      time step = 0.5
      transient step type = fixed
      time integration rule = implicit
      Predictor Rule is  forward euler
    end parameters for calore region calore

    begin parameters for adagio region adagio
      time increment = 0.5
    end parameters for adagio region adagio
  end time stepping block p2

  begin time stepping block p3
    start time =  10.0
    begin parameters for calore region calore
      time step = 1.0
      transient step type = fixed
      time integration rule = implicit
      Predictor Rule is  forward euler
    end parameters for calore region calore

    begin parameters for adagio region adagio
      time increment = 1.0
    end parameters for adagio region adagio
  end time stepping block p3

  termination time = 30.0

end time control

coupling region order = calore_adagio
coupling direction = one_way

##########################################################################
#                                        #
# CALORE Region                                  #
#                                        #
##########################################################################
```

```
begin calore region calore

   Use Finite Element Model mesh1 Model Coordinates are model_coordinates
   Use Linear Solver solve_temperature

   Begin Initial condition ICblock_0
    temperature = 293.0
    add volume block_100
   End

   Begin Results Output Label diffusion output
    Database Name is cone_pre-form_th7.e
    Nodal Variables = temperature as TEMP
    At Step 0, Increment = 1000
   End

   Begin Heat Flux Boundary Condition q_in
            Element Subroutine is moving_q
    Real Data 0.02 0.02 8.0 0.6 0.71 0.35 0.0
    add surface surface_101
   End

   Begin Convective Flux Boundary Condition on top-sides
    add surface surface_101
#     add surface surface_102
            add surface surface_103
            Convective Coefficient is 5.0e-2        # W/K-cm^2
            Reference Temperature is 293.0
#            Integrated flux output topflux
   End

#    Begin Radiative Flux Boundary Condition on top-bottom
#     add surface surface_101
#     add surface surface_102
#            Emissivity is 0.50
#            Reference Temperature is 293.0
#            Radiation Form Factor is 1.0
#    End

 end calore region calore

 ##########################################################################
 #                                        #
 # ADAGIO Region                                #
 #                                        #
 ##########################################################################
```

```
  begin adagio region adagio

    use finite element model mesh1

    options = thermalstrain

    ##########################################################################
    #                                        #
    # output definitions                          #
    #                                        #
    ##########################################################################

#     begin user output

#       node set = nodelist_101

#       compute global force_x as sum of nodal reactions(1)
#       compute global force_y as sum of nodal reactions(2)
#       compute global force_z as sum of nodal reactions(3)

#     end user output

    ##########################################################################
    #                                        #
    # history output                              #
    #                                        #
    ##########################################################################

#     begin history output houtput

#       database name = cone_pre-form.h
#       database type = exodusII

#       at step 0  increment = 1

#       variable = global force_x as force_x
#       variable = global force_y as force_y
#       variable = global force_z as force_z

#       variable = global kineticenergy  as kine
#       variable = global internalenergy as inte
#       variable = global timestep       as tstep

#       variable = nodal displacement at node 35 as displ
```

```
#    end history output houtput

    ########################################################################
    #                                                                      #
    # plot output                                                          #
    #                                                                      #
    ########################################################################

    begin results output output_adagio
     database name = cone_pre-form_me7.e
     database type = exodusII
     at step 0 increment = 1
#      nodal variables   = force_external       as f_ext
#      nodal variables   = velocity             as vel
      nodal variables   = displacement         as displ
      nodal variables   = temperature          as temp
      element variables = rotated_stress       as stress
              element variables = von_mises         as vonmises
              element variables = MAT%thermo_ep_power(1) as eqps
              element variables = MAT%thermo_ep_power(2) as radius
    end results output output_adagio

    ########################################################################
    #                                                                      #
    # Mechanical Boundary Conditions                                       #
    #                                                                      #
    ########################################################################

#    begin fixed displacement
#      node set = nodelist_104
#      component = z
#    end fixed displacement

#    begin fixed displacement
#      node set = nodelist_104
#      component = x
#    end fixed displacement

#    begin fixed displacement
#      node set = nodelist_104
#      component = y
#    end fixed displacement

    ########################################################################
    #                                                                      #
    # Solver definition                                                    #
```

```
    #                                                          #
    ############################################################################

    loadstep predictor using line search type secant

    begin adagio solver cg
      target relative residual = 1.0e-3
      maximum iterations = 10000
      minimum iterations = 0
      orthogonality measure for reset = 0.1
      line search type secant
      preconditioner = elastic
    end adagio solver cg

  end adagio region adagio

 end calagio procedure Cal_Procedure

  User Subroutine File is qflux-moving.f

end sierra cone pre-form test
```

Subroutine qflux-moving.f

```
      SUBROUTINE MOVING_Q ( FACEID, NELEMF, NINT, COORDS, T,
     &                  FLUX, IERROR )
      INTEGER FACEID, NELEMF, NINT, IERROR
      DOUBLE PRECISION COORDS, T, FLUX, RDAT(7)
      DOUBLE PRECISION TIME
      DOUBLE PRECISION pi, x0, y0, a0, b0, pwrmx, abp, qmx,
     &  time1, time2, x1, y1, xx, yy, rx2, ry2, vel, omega, d, r, dist,
     &  time_total
      DIMENSION FACEID(NELEMF)
      DIMENSION COORDS(3, NELEMF, NINT)
      DIMENSION T(NELEMF, NINT)
      DIMENSION FLUX(NELEMF, NINT)
C*************************************************************
C Set the heat flux on the surface as a function of the
C surface coordinate, using real data parsed from the
C input file.
C*************************************************************
      INTEGER INTPT, FACE

C*************************************************************
      CALL ACAL_GET_INSTANCE_REAL_DATA( 7, RDAT )
```

```
      CALL ACAL_GET_TIME(TIME)

       pi = 3.14159265

C  1/2 of the major and minor axis of the ellptical spot (cm) (a0=b0 for circle)
       a0 = RDAT(1)
       b0 = RDAT(2)
C  TOTAL POWER INPUT (W):
       pwrmx = rdat(3)
C  absorption (nd)
       abp = rdat(4)
       qmx = pwrmx*abp / (pi*a0*b0)
C  velocity of beam (cm/s):
                vel = rdat(5)
C  diameter of beam path (cm):
                d = rdat(6)
C  calculate needed parameters:
                r = d/2.0
                omega = vel/r
                dist = pi*d
                time_total = dist/vel

C  set time interval for power to turn on (sec):
       time1 = rdat(7)
       time2 = time1 + time_total

      if (TIME .ge. time1 .and. TIME .le. time2) then

       DO 20 INTPT=1,NINT
        DO 10 FACE=1,NELEMF
c         FLUX(FACE,INTPT) = 0.0
                  x0 = r*cos(omega*TIME)
          y0 = r*sin(omega*TIME)
          x1 = COORDS(1,FACE,INTPT)
          y1 = COORDS(2,FACE,INTPT)
                  xx = (x1 - x0) / a0
                  yy = (y1 - y0) / b0
                  rx2 = xx**2
                  ry2 = yy**2
          IF (rx2 .le. 1.0 .and. ry2 .le. 1.0) then
            FLUX(FACE,INTPT) = qmx * exp(-rx2) * exp(-ry2)
                   ENDIF
  10     CONTINUE
  20    CONTINUE

      endif
```

```
ERROR = 0
RETURN
END
```

DISTRIBUTION

2 Pennsylvania State University Electro Optics Center
222 Northpointe Blvd.
Attn: Tom Lehecka
Freeport, PA 16229

2 The University of Florida
Department of Mechanical and Aerospace Engineering
Attn: Gloria Wiens
Gainesville, FL 32611-6300

2 North Carolina State University
Department of Electrical and Computer Engineering
Attn: Eddie Grant
Engineering Bldg II (COE II) 3078, Box 7911
NCSU Campus
Raleigh, NC 27695

2	MS9018	Central Technical Files	8944
2	MS0899	Technical Library	4536
1	MS0123	D. Chavez, LDRD Office	1011
1	MS1064	J. Palmer	2455
1	MS1245	T. Gardner	2455
1	MS1064	S. Lott	2614
1	MS1064	F. Peter	2614
1	MS0889	G. Knorovsky	1813
1	MS0889	D. MacCallum	1813
1	MS0826	C. Wong	1513
1	MS0372	W. Scherzinger	1524
1	MS1454	M. Steyskal	2554